2014

An Assessment Of Available Hydrokinetic Energy Of The Gulf Stream Near Cape Hatteras, North Carolina

Asif Kamal Kabir
North Carolina Agricultural and Technical State University

An Assessment of Available Hydrokinetic Energy of the Gulf Stream near Cape Hatteras, North Carolina

Asif K.M.R. Kabir

North Carolina A&T State University

A dissertation submitted to the graduate faculty

in partial fulfillment of the requirements for the degree of

DOCTOR OF PHILOSOPHY

Department: Mechanical Engineering

Major: Mechanical Engineering

Major Professor: Dr. Arturo Fernandez

Greensboro, North Carolina

2014

The Graduate School
North Carolina Agricultural and Technical State University
This is to certify that the Doctoral Dissertation of

Asif K.M.R. Kabir

has met the dissertation requirements of
North Carolina Agricultural and Technical State University

Greensboro, North Carolina
2014

Approved by:

Dr. Arturo Fernandez Major Professor	Dr. Ronald Steed Committee Member
Dr. Mannur Sundaresan Committee Member	Dr. Adrian Cuc Committee Member
Dr. Trisha Sain Committee Member	Dr. Samuel Owusu-Ofori Department Chair

Dr. Sanjiv Sarin
Dean, The Graduate School

Biographical Sketch

Asif K.M.R. Kabir was born at Dhaka, Bangladesh in 23rd December, 1984, to Dr. Abul K.M.S. Kabir and Mrs. Anwara Begum. He earned his Bachelor of Science in Mechanical Engineering from Bangladesh University of Engineering & Technology in 2007. Between 2008 and 2010 he served as a faculty member at Daffodil International University. In 2010 he joined the doctoral program in Mechanical Engineering at North Carolina Agricultural & Technical State University. His undergraduate research was concentrated on experimental investigation of a double pipe heat exchanger with the inner pipe having a corrugated cross-section. Currently he is a candidate for Doctor of Philosophy degree in Mechanical Engineering from North Carolina A&T State University, Greensboro, North Carolina, USA. Mr. Kabir conducted his doctoral research on assessing ocean current energy in the Gulf Stream near Cape Hatteras.

Dedication

I dedicate my current research work to my parents, Dr. Abul K.M.S. Kabir and Mrs. Anwara Begum, who always inspired me in achieving higher academic excellences.

.

Acknowledgements

I would like to express my heartiest gratitude to the individuals who always encouraged and supported me both professionally and personally in completing this work. First and foremost, I would like to thank my academic advisor Dr. Arturo Fernandez, who has also been my research supervisor. Admittedly, without his continuous support, encouragement, patience and invaluable advice, this work would not have been at its current state. I greatly acknowledge to my committee members Dr. Mannur Sundaresan, Dr. Ronald Steed, Dr. Trisha Sain, and Dr. Adrian Cuc for reviewing my effort and suggesting many constructive recommendations.

I expressed my sincerest gratitude to Department of Mechanical Engineering for the opportunity for the opportunity I was given initially through the enrollment in this program. I would also like to express my gratitude towards the Coastal Studies Institute of the University of North Carolina for their financial support throughout. I greatly acknowledge these organizations for their financial and technical support to accomplish this research work.

Finally, I would like to convey my deepest appreciation to my parents, Dr. Abul K.M.S. Kabir and Mrs. Anwara Begum, my wife Ragina Rafiq, and other family members for believing in me. Their consistent mental support, love, and affection always played a significant role in my journey in life.

TABLE OF CONTENTS

List of Figures

List of Tables

Abstract

Ocean currents have the potential to supply electricity from a renewable source to coastal regions. The Gulf Stream, part of the North Atlantic Gyre, flows parallel to the Southeastern coast of the United States and could potentially supply a significant electricity to this region. The assessment of the potential energy that could be generated is the first step towards developing this resource. Data from the HYbrid Coordinate Ocean Model (HYCOM) and high-frequency radar measurements have been used to assess an area extending from 34.85° N to 35.15° N, and from 74.85° W to 74.5° W near the North Carolina shore. The assessment shows the area to be a promising resource of renewable energy as over 50% of the days exhibit a power density of 500 W/m^2 or higher. The results also show the direction of the ocean velocity to be relatively uniform in the Northeast direction, which would facilitate a future exploitation of the resource. Statistical analysis applying Probability Density Functions (PDF) such as Weibull, Rayleigh, and Gaussian distribution is introduced in the field of ocean current energy. The results show that the use of a Weibull probability distribution facilitates the analysis of ocean velocity conditions. Weibull distribution is also able to predict the power density with a high degree of accuracy. The analysis was also expanded to other gyres with similar results, where the Weibull distribution is the better predictor for power density.

CHAPTER 1

Introduction

The global demand of energy consumption is increasing every year, which is directly proportional to the trend of the economic development of a country. This trend in economic growth also brings with it some disadvantages. One of the primary negative impacts that increased energy consumption has on the environment is its detrimental impact on the global climate. This negative effect is directly proportional to the amount of non-renewable energy sources that has been used for power production. These non-renewable energy resources are responsible for emitting pollutants and greenhouse gases which directly impact our climate (Vanek & Albright, 2008). A major source of non-renewable energy is fossil fuels such as oil, natural gas, and coal. This has created a need for energy sources other than fossil fuels.

During the 1960s and 1970s, nuclear energy started to become a popular avenue in the power sector due to the high amount of energy production. The investment in this sector was increasing every year until the mid-1980s. During that period nuclear energy provided nearly 19% of the total energy produced in the U.S. (EIA, 2013; see Figure 1). But ever since some catastrophic environmental disasters (e.g., Chernobyl in 1986, Fukushima Daiichi in 2011) involving nuclear power plants, interest in this sector started to decline. In addition to the high safety precautions needed, the difficulty in processing the nuclear wastes has also made it a less popular source of energy. This cause and effect has prompted governments to look for alternative renewable energy resources that will not only solve the energy problem but also ensure a pollution-free environment for future generations.

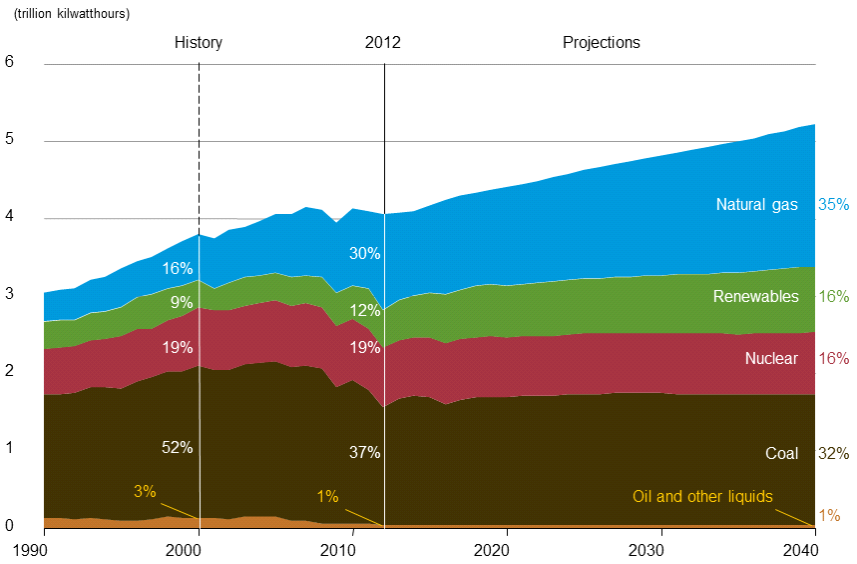

Figure 1. Percentage contribution of different sources of energy in total power generated (1990-2012) and total power to be generated (2013-2040) at United States (EIA, 2012).

The availability of a renewable energy source does not ensure the solution to energy demands. The available energy needs to be studied in order to determine whether the source of potential energy is socially and economically practical in its endeavors, and must be analyzed to fit three primary criteria—the amount of energy available for extraction, the cost of extraction of power, and the environmental impact of the extraction of power. The primary question that needs to be answered is whether the amount of available power is good enough to be extracted. Therefore, an assessment needs to be conducted that will give a detailed overview of the energy condition prevailing in the area of interest while providing reliable data.

1.1 Energy Situation in the United States

The United States is the second largest consumer of energy with China also leading the charts of being largest energy producers (EIA, 2014). About 68% of this energy produced comes from fossil fuel resources (see Figure 1). The U.S., with 11,110 barrels/day, is also the second largest producers of oil in the world behind Saudi Arabia. However, the high consumption rate of

approximately 18,490 thousand barrels/day creates a huge shortage of oil. This shortage is balanced with import of oil which thus results in a significant increase in the total cost of energy consumption.

The United States is also the leading consumer of natural gas in the world with the total consumption in 2012 increasing by 4.1% compared to the previous year (BP, 2013). The continuous increase of usage of these resources for energy production is resulting in increased CO_2 emission with local governments of different states getting more concerned about this emission into the atmosphere. State governments are starting to take preventive actions with nine of the northeastern states combining to form the Regional Greenhouse Gas Initiative (RGGI). The primary task of RGGI is to set regulations of maximum allowable CO_2 emission by the energy production companies. RGGI is performing this task by reducing this maximum allowable emission every year to bring the climatic condition to a much more sustainable state. In 2013, the state of California also took similar initiatives and formed California's Cap-and-Trade program (Center for Climate and Energy Solutions [C2ES], 2014) with an initial goal of reducing CO_2 emission by 16% by 2020. These initiatives will act as a stepping stone for the renewable energy sector to start replacing fossil fuels as an energy source.

1.2 Energy Situation in North Carolina

Regions around the world that have rich reserves of fossil fuel have benefited from the abundances of these commodities and have prospered well using these resources. The state of North Carolina is not one of them and does not have any fossil fuel resources. This has not stopped the development of this region although the progress accompanies with it a large cost. Of the total power produced in North Carolina in 2011, around 63% came from natural gas and coal combined, while 31% was from nuclear power plants (EIA, 2013). During this period, only

6% of the power produced came from using renewable resources with biomass and hydropower contributing to almost all of it (EIA, 2012). As most of the energy consumed comes from fossil fuels, the state has to import these fuels from outside to meet the energy demands. This impacts the overall expenditure with an increase in the per capita cost of energy production. Thus the cost of producing power in North Carolina depends upon factors which are not dictated within the state. Subsequently, a source of energy that originates within the state will not only decrease the cost of power production but will also increase the reliability on a continuous supply of power.

1.3 Types of Renewable Energy

Energy sources that are being continuously restored on a certain cyclic order are termed as renewable energy. Renewable energies include solar, wind, and hydroelectric power. Renewable energy resources are not only useful in improving the environment but they also ensure a sustainable source of energy for the locality in which it is harnessed.

The sun is the primary source of all the available renewable energies, and all other renewable energy sources are in one way or another dependent on it. The U.S. Department of Energy (US DOE, n.d.) emphasizes the investment of solar power, reflected by the number of Solar Energy patents related to the DOE between 1975 and 2008. This is more than any other institution of the world (US DOE, n.d.). With the decrease of installation costs (more than 30% between 2008 and 2012 [US DOE, n.d.]), and in addition to commercial installations, it is also becoming popular among domestic applications. It was estimated that solar panels, with a capacity of more than 3300 megawatts, were expected to be installed in the U.S. in 2012, which was more than double the amount that was installed in 2011 (Sweet, 2012). Although a source of clean energy, solar energy is not free from demerits. In addition to the large amount of

continuous space required for commercial power production, its ineffectiveness during the night makes it complicated to use it for base load power production. This results in large sized batteries used for storage in order to use power during the night time. This means that even though the energy itself is clean, the use of batteries with lead content and sulfuric acid make it a less beneficial prospect for the environment.

The most popular technique of power production using renewable resources is wind energy. It can be harnessed both on-shore and off-shore but also requires large amounts of space for the entire setup. Unfortunately, the necessary conditions are only found e in the mountains and coastal areas of North Carolina, which are also very popular tourist attraction destinations.

Occupying approximately 70% of the total surface area of the world, the world's oceans are a potential source of renewable energy in both mechanical and thermal form. An ocean can be described a reservoir of salinized water in a turbulent state driven by the forcing of wind and thermo-haline circulation. The entire oceanic system is governed by the conservation laws of mass, momentum and energy. The current contribution of the ocean to the production of energy throughout the world does not measure to its vast resource possibilities. Technologies harnessing energy from the oceans include 'Ocean Thermal Energy Conversion (OTEC)' systems, wave energy, tidal energy and extraction of hydrokinetic energy from the continuous flow of ocean currents. The harnessing of energy using temperature gradient, wave energy, and tidal energy have all gone into production level, in some cases into commercial level, whereas harnessing energy from ocean currents is still in its preliminary stage.

1.4 Ocean Current as Renewable Energy

An ocean current is a unidirectional, continuous flow of water resulting from the balance between Coriolis forces, thermohaline circulation, and tides. Ocean currents vary in size and

strength with the large ones even impacting Earth's global climate. For example, the Gulf Stream, which flows beside the eastern boundary of the United States and the western boundary of Europe, is responsible for the warm climate in Western Europe. The large ocean currents that flow around several thousand miles also involve large flow-rates. An example is the Florida Current which has a volume flow-rate thirty times greater than all the rivers of the world combined (Smentek-Duerr, 2012).

The strongest ocean currents are known as ocean gyres. These gyres are usually located in the large ocean basins of the world. The five major gyres are the Indian Ocean Gyre, North Atlantic Gyre, North Pacific Gyre, South Atlantic Gyre and South Pacific Gyre. Part of the North Atlantic Gyre, called the Gulf Stream, has been subjected to numerous research due to its geographic location and the impact it has on the global climate.

1.4.1 The Gulf Stream. The Gulf Stream swiftly flows from the eastern side of the Gulf of Mexico through the Florida Straits, and then parallels to the southeastern coast of the United States up to North Carolina. After reaching Cape Hatteras, the northward Stream bends eastward into deeper water towards Europe (see Figure 2). And because it is far enough away from the coast of North Carolina, into the deep waters, it does not have the disadvantage of power extraction through the disturbance of the local inhabitants.

During the 1970s, oil prices started to rise and people became more conscious about a pollution-free environment. Some initiatives looked into the prospects of ocean current as a source of clean energy. Scientists and researchers began to consider it as a long term viable option (Duerr & Dhanak, 2012). By the early 1980s, and since the price of oil began to decrease, the interest in ocean current as an energy prospect waned. In the last decade, however, the interest in renewable sources of energy has increased. As a promising source of energy, the Gulf

Stream has caught the attention of scientists and oceanographers. Part of this stream that passes through the Straits of Florida, also known as the Florida Current, has been subjected to numerous interests due to the shallow water depth and closer distance from the shore of the location. However, few works are available regarding the assessment of power further downstream of the Florida Straits near Cape Hatteras where the transport almost triples (93Sv, 1 Sv = 10^6 m^3/s) compared to the Straits (32Sv) (Duerr & Dhanak, 2012; Leaman, Johns, & Rossby, 1989).

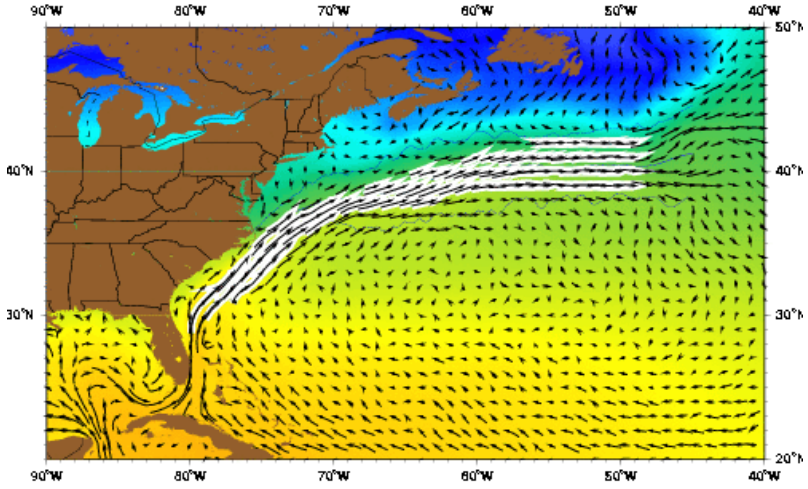

Figure 2. Surface current of the Gulf Stream near North Carolina. Source: http://oceancurrents.rsmas.miami.edu/atlantic/gulf-stream_3.html

1.5 Purpose of Study

Assessment of a particular energy, at a given site, evaluates the prospect by harnessing the energy using power extraction devices. Even though the amount of power available per unit area, also known as Power density (P_d), is the primary tool for assessing energy resource originating from fluid flow, the directional variation of the flow also plays its part. The seasonal variation of the flow is also important due to the need for continuous availability of power throughout the year.

Considering the amount of energy that can be extracted due to the increased transport near Cape Hatteras, this region is investigated to assess the overall prospect. The primary aim is to conduct a complete statistical analysis of the resource in order to evaluate the potential energy that could be extracted. In addition to the methods that have already been used to study ocean current energy, a set of statistical tools are introduced in this study that are compared with each other to analyze the best possible tool that can be used for future studies. The assessment starts with determining the probability density distribution (PDD) of the ocean current speed, which determines the performance of ocean current energy at a certain location within the time range (Celik, 2004). PDD is also useful for the prediction of economic viability of setting up the entire project. Once the PDD is known, the energy condition of the site based on available data can easily be obtained. Probability density functions (PDF) are then introduced which are used to mathematically model the PDD for predicting the power density and eventually the energy prospect of the given site. The convenience in using a mathematical model rather than a set of data acts as an advantage for using PDF.

1.6 Overview of Dissertation

This research presents an improved approach to ocean current energy resource assessment by using statistical tools. The dissertation begins in Chapter 2 with a comprehensive literature review in renewable energy, with more emphasis given on ocean current energy, particularly in the Gulf Stream. Recent progresses are discussed here along with the developments of the team from Florida Atlantic University. The third chapter emphasizes the methodology of the study, which starts with the introduction of statistical tools used for the assessment process. These tools are used for assessing the energy condition of the Gulf Stream near Cape Hatteras using nine years of data from an ocean current model, which is called the

Hybrid Co-ordinate Ocean Model, also known as HYCOM. The assessment is conducted at a predetermined site that is deemed an adequate location for harnessing energy through initial assessment, which is selected by the Coastal Studies Institute at the University of North Carolina as a part of a project funded by the state of North Carolina. A comparative method to determine the best possible location for installation of hydrokinetic energy extraction devices are also described in this chapter. Chapter 4 mainly focuses on the assessment of the area of interest using the statistical tools introduced in the previous chapter. After applying the statistical tools selected for analysis, the results obtained are compared to evaluate the tool which can more accurately describe the ocean current. This chapter also includes the results obtained from the assessment process. In Chapter 5, the results obtained from the assessment are discussed in detail and they are analyzed to determine the possible outcomes. This chapter also concludes the dissertation and suggests future work for further improvement on ocean current energy assessment.

CHAPTER 2

Literature Review

2.1 Renewable Energy

The use of energy, by means of renewable resources, dates back to as early as 200 B.C (Williams, 2013). During this time Europeans developed the idea of using a vertical watermill for harnessing energy that free flowing water possesses. Not only was this energy used for domestic purposes, such as crushing grains and tanning leather, but harvesting this kind of energy represented systems of economic and industrial prosperity (Williams, 2013). Eventually, hydropower technologies reached the next step of energy yielding. During the middle ages, dams were built to store and develop water pressure to operate the water mills that were built around bridges and boats (Williams, 2013). Use of water power as a source of energy took a large step during the fifteenth century. Development of mechanical components like the camshaft and crankshaft initiated the large scale application of water power in the iron industry. The use of wind power as a source of energy also developed during a similar time frame (Wilburn, 2011). In 200 B.C., people in China began using wind-driven mills for pumping water; and by the end of 11th century this technique was being used for grinding grains in the Middle East.

Even though speculations exists about Romans being the first civilization to use sunlight as a mean of energy, the first significant step taken for using solar energy was made by a French engineer named Augustine Mouchot (Perlin, 1999). His penchant for solving the future energy problem led him to build an experimental setup for trapping solar energy, which is more commonly known as the green house. Unfortunately the location of his setup and the inability to

operate the day long cycle resulted in his failure to establish the technology; however, it did act as a stepping stone for future experimental study.

2.2 Renewable Energy in United States

During the early part of the 20th century, Frank Shuman started working on solar energy prospects from where Mouchot had left off. He started to study the reasons for failure of Mouchot's project (Perlin, 1999). In his Pennsylvania backyard, Shuman was successful in building a model that was used for driving vapor-operated engines using solar energy. The success of his setup encouraged him to conducting further study. He expanded his entire operation to Egypt where he also introduced a storage system for warm waters which could be used during night. His entire project was a success and this was the first time the application of solar energy proved to be more cost-effective compared to the available energy options.

The first significant addition to the study of renewable energy in the United States occurred in 1880. In Grand Rapids, Michigan, at the Wolverine Chair factory, a water turbine was coupled with a dynamo, for the first time, to produce electricity for illuminating street lights. This marked the beginning of an era of supremacy of Hydro power in the United States. This development provided 15% of the total supply of electricity, with the figure rising as high as 40 percent of the total production by the early 1940s (Energy n.d.). Hydropower still constitutes a large portion (10% in 2003) of the total power production, with the conventional capacity in the United States nearly tripling (U.S. Department of Energy, n.d.).

During the early part of 1970's the symptoms of oil emergency were slowly starting to be revealed in the United States. A small number of domestic reserves resulted in the decrease of imported gasoline. The situation became worse after the embargo was imposed the Organization of the Petroleum Exporting Countries (OPEC); it resulted in not only a huge price hike in the

price of oil in the United States, but also a great shortage of supply (The History Channel, 2014). This resulted in the "Energy Policy and Conservation Act" being introduced in 1975 with renewable energy resources development occupying a large share.

2.3 Various Forms of Ocean Renewable Energy

The ocean is a vast source of renewable energy and can take various forms including thermal gradients, waves, tides, offshore wind and ocean current. The prospect of this ocean resource can make a significant contribution to the energy sector of coastal regions. Although only a fraction of these ocean energy resources has been utilized thus far, predictions have been made that these resources will be contributing nearly 7% of the world's total energy needs by the year 2050 (Esteban & Leary, 2012). Being predicted to be a large part of the future energy production, the current status of the utilization of these various forms of ocean renewable energy is described in the following subsections.

2.3.1 Offshore wind energy. Unlike onshore wind energy converters, which have been utilized for a long time in various purposes, the idea of offshore wind farms only materialized less than 3 decades ago. Although utilizing offshore wind energy have more prospect because of the lower surface roughness and lesser visual obstacles for free flowing air, the primary obstacle for achieving success in this field was the inadequate technological development for setting up and maintaining such a collection of structures in the middle of the ocean. These obstacles were finally overcome during the early 1990s, when the first offshore wind park of nearly 5 MW capacity started operating in Denmark. Since then, Europe has become the leading region in the world energy industry in construction and development of off-shore wind farms.

In the United States, the potential of offshore wind energy has had some extra barriers to overcome compared to Europe. The ocean along the coastline of the U.S. is not only deeper than

Europe, but the climate conditions are also more severe. These conditions add more constraints for the design of the turbine structures and mooring systems. Such obstacles did not hold back in taking initiatives for assessing this sector. There are currently 13 off-shore wind energy projects at an advanced stage, getting at least State or Federal approval, with the Cape Wind project of Massachusetts becoming the first commercial project in 2010 to receive federal clearance for establishment (Musial & Ram, 2010).

The National Renewable Energy Laboratory (NREL) recently prepared a report assessing the total offshore wind energy prospects in the U.S (Schwartz, Heimiller, Haymes, & Musial, 2010). The report also entailed individual prospects of 27 different states along the coastline of the U.S., including North Carolina, with available power of 300 GW. Even though the assessment process had some inbuilt error causing some under-prediction (Smentek-Duerr, 2012); if a fraction of the 4,150 GW of available power in the offshore winds of U.S. can be harnessed, it could potentially mean a significant contribution to the national power supply.

2.3.2 Ocean thermal gradient. Ocean Thermal Energy Conversion (OTEC) utilizes the temperature gradient present in the ocean between the warm sea surface and the cold deep water. The temperature difference usually ranges between 10~25^{o} C, but this temperature gradient is usually higher in equatorial and tropical waters (Rajagopalan, 2013). OTEC devices are run on a Rankine cycle and used for base-load plants for their 24 hour availability. The efficiency of an OTEC plant may also depend upon bottom topography and a profile of the seabed, with currents, waves, climate conditions, and chemical composition of the sea-water at the area of interest also having their share of influence (Uchida, 1983). Based on the working principle, OTEC systems are primarily of two types: open cycle, where the working fluid is sea water, and closed cycle, where fluids with low boiling points like ammonia and R-134a are used as working fluids.

The global prospect of 30 TW for OTEC (Rajagopalan, 2013) of which even if a slight fraction can be harnessed can contribute a big portion of Worlds energy demands. The U.S. government took the first initiative in this sector during the early part of 1980's; the Natural Energy Laboratory of Hawaii Authority (NELHA) set up a closed-cycle Mini-OTEC in Hawaii(OTEC International 2011). Although this technology has been tested in modeled size and has been built for small amounts of power production, it still has not gone on to commercial level. Recently plans have been taken to develop a 10 MW plant in China, while the state of Hawaii is planning to build an OTEC facility with a 100 MW capacity.

2.3.3 Wave energy. The oscillation of water particles created by wind flowing over the ocean's surface is known as waves. Waves differ based on frequencies and wavelengths which is dictated by wind speed and the friction of the ocean surface. The amount of energy that is considered available depends primarily upon the frequencies and the amplitudes of the waves. Therefore, regions with the depth of around 40 to 100m are considered optimal for energy extraction, as these regions are not shallow enough for the waves to have interactions with sea-beds while also not deep enough to increase substantially the installation, maintenance and transmission costs (Scruggs & Jacob, 2009).

Wave energy primarily consists of two parts: potential energy resulting from the height of the waves and kinetic energy which is due to the motion of the waves. The total energy, which is the primary tool for assessing wave energy, is directly proportional to the period of the waves(T) and square of the wave heights(H^2) measured from the following equation (Minerals Management Service, 2006):

$$P = \frac{\rho g^2 T H^2}{32\pi}, \quad (1)$$

where ρ is sea-water density and g is the gravitational acceleration. The initial step of the assessment process for the harnessing of wave energy is to calculate the wave height and the period of waves. Based on the current technologies available, wave energy extraction devices are available based on four different types of working principles: point absorbers, attenuators, terminators, and overtopping devices (Minerals Management Service, 2006).

The U.S. Electric Power Research Institute (EPRI) recently estimated the overall availability of wave energy along the coasts of United States to be in the region of 2640 TWh/yr, which is around 26% greater than the previous estimate they conducted in 2004 (Jacobson, Hagerman, & Scott, 2011). A major portion of this increase was seen on the East Coast (including shores of NC) where the estimate increased by 82% (Jacobson et al., 2011). In spite of having such a good prospect, its presence near the shores with is a probability of large interaction with human habitat makes it a difficult proposition to consider.

2.3.4 Tidal energy. The major difference between tides and waves is the nature of their driving force. As waves are generated by forcing of the wind flowing over the ocean, tides are usually driven by the gravitational pull resulting from the relative position of the Earth, the Moon and the Sun. Thus tidal energy are more predictable depending primarily upon Earth's constant rotation compared to dependence of wave energy on the more unpredictable climate dependent wind forcing. The most common method of utilizing the tidal energy resource is by storing water in a barrage during the high tides and letting the water go through a turbine during the low tides. This technology was used for the first ever tidal power station built in France. The facility built on the La Rance river estuary in 1965 has a capacity of 240 MW (EPRI report). The same methodology for energy extraction were later followed for a 500 kW capacity project built in Russia and a 20 MW plant built I 1980s at Annapolis Royal, Nova Scotia (EPRI report).

In addition to using tidal energy as source of potential energy, it also can be used as a kinetic energy source. In this case energy available will be governed the equation which same as wind energy. In comparing the energy potential of the wind and the tides, the low velocity of the tides are usually balanced by the much higher density values of water compared to air. But there still remains a drawback in extracting tidal energy. Although tidal energy are more predictable, the fact that in most of the coasts the tidal cycle consists of four phases a day (in some places two) makes it a difficult resource that can be used for energy extraction for base loads.

2.3.5 Ocean current energy. An ocean current is a large structure of circulating ocean water flow with the Coriolis Effect acting as the primary driving force. The other forces that also have an influence are temperature and salinity gradients, tides, winds, the gravitational pull from the sun and the moon, etc. These ocean currents primarily vary in size with large ocean currents existing in large oceans travelling past the boundaries of the continents. The continuous flow of the ocean water and their unidirectional nature make the ocean currents an exciting source of extracting power.

One of the novel ideas that surfaced as a source of renewable energy after the oil crisis in the early part of 1970s was utilization of ocean current. People occupying the decision-making and administrative positions were looking for every kind of opportunity to solve this sudden energy crisis. Initial interests were centered on the part of the Gulf Stream that comes through the Florida Straits, also known as the Florida Current, due to the suitable location compared to the shore for energy extraction. Von Arx (Von Arx, Stewart, & Apel, 1974) estimated the available power for extraction to be in the region of 25 GW. Out of this amount, the actual quantity that can be extracted varied between 1 GW and 10 GW, according to different researchers (Smentek-Duerr, 2012). Von Arx's suggestion was limited to 1 GW only because he

suggested that extraction of more than 4% of the available power will impact the climate conditions of the region. On the other hand Lissaman, who studied several models, suggested that extracting 10 GW of power from the Florida Current will only impact the current velocity by 1.2%, a much lesser impact than the natural fluctuation of the velocity.

One of the unique benefits of the Gulf Stream is the increase in transport of the stream as it goes further away from the Straits along the eastern coasts of the United States. Leaman et al. (1989) studied the volume transport of the Gulf Stream at three different sections, which included the Florida Straits and a location near Cape Hatteras in this regard. They came to the conclusion that the flow-rate, which is 32 Sv in the Gulf Stream near the Straits, almost triples (93 Sv) as it reaches Cape Hatteras. Ichikawa and Beardsley also conducted similar studies during the early 1990s in the Kuroshima current (Ichikawa & Beardsley, 1993). They found the mean transport to be around 23 Sv during their study. Marais, Chowdhury, and Chowdhury (2011) introduced the term Significant Impact Factor or SIF usually used for assessing tidal energy in ocean current energy assessment (Marais et al., 2011). SIF, which indicates the amount of attainable power without significantly affecting the continuity of the flow, was proved to be more than tidal energy prospect as the ocean current can get back to its original shape quicker than tidal energy projects due to presence of more open boundaries. Duerr and Dhanak (2012), in a study to examine the prospect of the Florida Current introduced a correlation equation for locating the best possible position for positioning energy extraction devices. Although the correlation is long way from getting a generalized form for finding the most optimum position, it still will act as an initial step for future studies.

.

CHAPTER 3

Methodology

3.1 Data Source

An assessment process starts with identification of the variables which are pertinent to the study (Smentek-Duerr, 2012). These are then collected over a period of time and thus analyzed to decide upon the outcome of the assessment. The primary source of energy in ocean currents, which follows a dynamics similar to channel flow (Smentek-Duerr, 2012), is the kinetic energy resulting from velocity of the currents. But the variability (both spatially and temporally) and complexity present in world ocean could not yet be overcome to have a stable and reliable onsite method to assess its potential (Yang, 2013). So ocean circulation models which are run by numerical analysis of the conservation equations which primarily governs different physical phenomenon of the ocean, still remains the most viable option of assessing any characteristics of world ocean. The current study also uses an ocean circulation model, Hybrid Coordinate Ocean Model (HYCOM), as the primary tool for assessment of ocean current energy.

3.1.1 Computational model data. The velocity data for this study have been collected from "HYCOM," an upgraded primitive equation ocean general circulation model of the Miami Isopycnic-Coordinate Ocean Model (MICOM) developed by Bleck and coworkers (Chassignet et al., 2007; Halliwell, 2002). Since its development, MICOM became a popular ocean circulation model especially for ocean climate studies (Halliwell, 2002). But MICOM was not free from any shortcomings. Its inability to utilize layers which were less dense than the mixed layer created the need for further development in ocean current modeling. This resulted in development of HYCOM which resolved the issues which MICOM could not deal with.

HYCOM is a three dimensional model with a horizontal resolution of 1/12° along the longitudinal direction and the temporal resolution is limited to daily averages (Chassignet, 2002; Halliwell, 2002). It computes salinity, temperature, eastward and northward components of velocities of the ocean current at a given location. The vertical resolution remains similar to MICOM in the open, stratified ocean while transitioning to sigma co-ordinate model in the shallow water region. In between of these two regions in the upper-ocean mixed layer, HYCOM follows z co-ordinate (constant depth) model for computation of the parameters. The pros and cons of using ocean current model already been discussed by Duerr (Smentek-Duerr, 2012).

The region at which the velocity data are collected covers 34.85° N to 35.15°N and 74.85°W to 74.5°W with the nearest point to the shore located 65 kilometers from Cape Hatteras. This location was chosen as part of a project initiated by Coastal Studies Institute of the University of North Carolina in collaboration with the State of North Carolina. The data have been analyzed at 16 different positions which are shown in Table 1. Table 1 also shows how these points are denoted in the remaining part of this literature. The data spanned between November 2003 and December 2012 and the position of the location is illustrated in Figure.3.

Table 1

Different Locations and their Notations

Latitude Values	Denoted by	Longitude Values	Denoted by
34.9	A	-74.8	1
34.96	B	-74.72	2
35.03	C	-74.64	3
35.09	D	-74.56	4

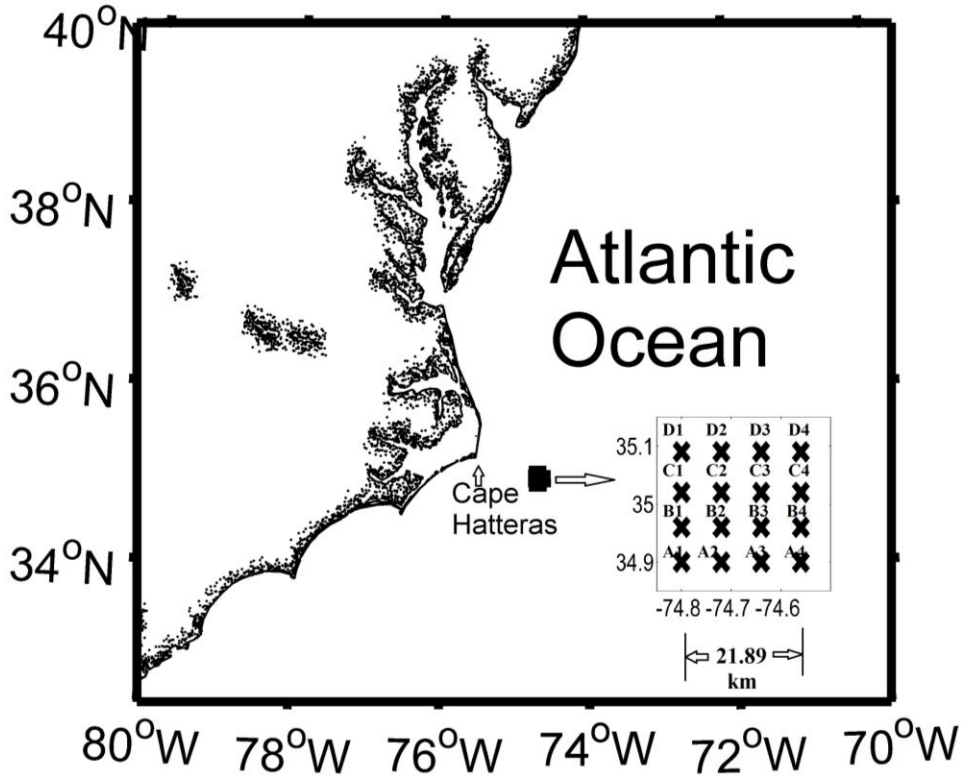

Figure 3. Geographical location of the area of interest.

3.1.2 Measured data. The Coastal Observing Research and Development Center (CORDC; CORDC, 2014) placed high frequency (HF) radars in the east and west coast of the United States. One of these HF radars in the Atlantic coast measures surface current velocity at 35.113°N ~74.7699°W which is near our point D1 spanning between 16th March 2012 and 15th March 2013. The measurements are available at http://hfrnet.ucsd.edu/thredds/catalog.html. Although this source has a better temporal resolution, with hourly averages being available, as a developing measuring technique only a fraction of data was available of a possible 24 for most of the days. To account for this, available hourly averages were converted to daily averages by taking the mean of available hourly averages of each day for the complete analysis.

3.2 Power Density

The assessment of any energy resource includes the quantification of the power which could be potentially extracted from the resource. When the resource involves kinetic energy from a stream, it is convenient to use the power density which can be derived from the equation of kinetic energy (KE). The KE of a moving fluid with mass m and velocity v_{ins} can be represented by the following formulae:

$$KE = 0.5 * m * v_{ins}^{2} \tag{2}$$

where, mass m is a product of the density and the volume of the fluid. As power represents energy per unit time, replacing the term of mass from equation 2 with expression of mass flow-rate ($\dot{m}$), represented in equation 3, will yield the power available(KP) due to kinetic energy (equation 4).

$$\dot{m} = \rho * A * v_{ins} \tag{3}$$

$$\mathrm{KP} = 0.5 * \rho * A * v_{ins}^{3} \tag{4}$$

Here, A is the swept area facing the flow and ρ is the density of the fluid.

But to describe the potential availability of energy that can be harnessed based on power will not give a proper view of the resources as the potential size (swept area) of the hydrokinetic power extraction devices will dictate the overall amount. So a more generalized parameter for computing the resource is the Power density (P_d), which can be determined by dividing the power available by the swept area. Power density in a fluid stream across a unit cross-section thus can be given by the expression:

$$P_d = \frac{1}{2} \rho v_{ins}^{3} \tag{5}$$

The variation of density in the ocean throughout the water column is very negligible throughout the water column. Thus the power density becomes a direct function of the cube of velocity of ocean current.

However, this power density equation is only good for calculating instantaneous values. It would not be feasible to use this equation for calculating mean power density ($P_{d,m}$) simply by using the time –average of the instantaneous velocities. As the power density is the function of cube of the velocity, slightest variation in the values of velocity will result in a significant variation in power density. So the use of average velocity (v_{avg}) for calculating average power density in equation (5) will result in under-prediction of the actual energy condition in the assessment site. To account for this under-prediction, an additional term involving average velocity and standard deviation (σ) is added to the power density correlation (Duerr & Dhanak, 2012; Hennessey, 1977; equation 6).

$$P_{d,m} = \frac{1}{2}\rho(v_{avg}{}^3 + 3v_{avg}\sigma^2) \tag{6}$$

3.3 Statistical Tools

The primary driving force behind using a statistical analysis for a given set of data is the presence of outcomes which are dissimilar to the ones supposed to occur (Kalbfleisch & Prentice, 2011). These outcomes, generally known as failures create setbacks which people do not like to face. Statistical analysis gives a scientific approximate indication of the possibility of facing such an outcome. From natural phenomenon to manufacturing process, from share market analysis and improving customer services to energy analysis, there is hardly any field that does not use statistical analysis. Depending on the type analysis required, a wide range of statistical tools are available. Statistical tools can be used for either a certain significant outcome or to assess a combined process to evaluate the end result.

3.3.1 Probability density function. The available power being a direct function of velocity does not ensure velocity as the only factor which governs the energy potential of a certain site. In addition to the velocity itself, the fraction of the total duration the high velocity lasts also plays an important part. Thus, in order to know the energy potential of certain site, it is imperative to know the instances over a period when the productive power is available in addition to the duration of time it lasts. So the probability of occurrence of each available ocean current velocity is very essential to study the prospect of a potential site (Saenko, 2008). The probability *P* of a certain discrete variable v_i can be represented by the following relation:

$$P\,(v_i) = \frac{n_i}{n} \tag{7}$$

where, n_i represents the number of observations of the discrete variable v_i and n represents the total number of observations available. But it is always not convenient to calculate the probability from a set of discrete values. When the total number of discrete data becomes very large, it is more suitable to describe the entire outcome using a mathematical formulation governed by a very limited number of parameters.

A common mathematical tool used for statistical analysis is a probability density function or PDF. It is a continuous mathematical function used to model time-series data. It describes the likelihood of observing a range of values out of a set of data such as ocean velocity and is often utilized in statistical analysis. Various types PDFs are available out of which the most commonly used is the Gaussian distribution. The Rayleigh and the Weibull distributions have been used in assessing wind energy projects as it has been shown to capture the statistical properties of atmospheric boundary layer (Lun & Lam, 2000; Safari & Gasore, 2010).

3.3.1.1 Weibull distribution. In the field of energy analysis, the two parameter Weibull distribution is the most popular PDF due to its simplicity and ability to fit a wide range of data.

One of its major limitations is its inability to deal with negative data. But this has not limited its application in wind energy sector, as its ability to fit wind velocities (Garcia, Torres, Prieto, & de Francisco, 1998; Hennessey, 1977), has made it a very useful tool in this field. The similarities in type and the theories in wind and ocean current energy has prompted the use of Weilbull analysis as the statistical tool in the present study for the statistical analysis of the ocean current velocity. The PDF of the two parameter Weibull distribution for a certain velocity value v_{ins} at any instant is represented by the following equation:

$$f(v_{ins}) = \frac{k}{c}\left(\frac{v_{ins}}{c}\right)^{k-1} \exp\left(-\left(\frac{v_{ins}}{c}\right)^{k}\right) \tag{8}$$

where 'c' is the scale parameter, 'k' is the shape parameter and $f(v_{ins})$ is the probability of observing v_{ins} at any instant.

Several analytical and graphical methods are available for calculating the values of these two parameters (Costa Rocha, de Sousa, de Andrade, & da Silva, 2012; Lun & Lam, 2000). One of these methods which have shown better results in estimating wind power potential is the Maximum Likelihood Estimate (MLE). In MLE method, which is used in the present study, the following iterative equations are solved for calculating the shape and the scale parameter (Costa Rocha et al., 2012):

$$k = \left(\frac{\sum_{i=1}^{N} {v_i}^{k} \ln(v_i)}{\sum_{i=1}^{N} {v_i}^{k}} - \frac{\sum_{i=1}^{N} \ln(v_i)}{N}\right)^{-1} \tag{9}$$

$$\mathrm{c} = \left(\frac{1}{\mathrm{N}} \sum_{\mathrm{i}=1}^{\mathrm{N}} {\mathrm{v_i}}^{\mathrm{k}}\right)^{1/\mathrm{k}} \tag{10}$$

where v_i is the speed at time step i and N is the total number of velocity data points. Another way method of expressing the probability of a variable is through the cumulative distribution function or CDF. CDF gives the probability of the variable being less than or equal to the

independent variable of the function. The Weibull cumulative distribution function (CDF) is represented by the following equation:

$$F(v) = 1 - \exp(-(\frac{v}{c})^k) \tag{11}$$

An advantage of describing a time series as a function of a PDF is that it allows us a straightforward quantification of power density. The Weibull parameters can also be used to measure the average power density for a given site using the following expression:

$$P_{d,w} = \frac{1}{2} \rho c^3 \Gamma(\frac{k+3}{k}) \tag{12}$$

where 'Γ' represents gamma function.

3.3.1.2 Rayleigh distribution. Another popular PDF used in the field of wind energy is the Reyleigh distribution. It is a special case of the Weibull distribution where the shape parameter is fixed as 2. This leaves only one parameter, which characterizes the Rayleigh distribution. The PDF of a Rayleigh distribution for a certain velocity value v_{ins} at any instant can be represented by the following formulae:

$$f(v_{ins}) = \frac{v_{ins}}{c^2} e^{-v_{ins}^2/(2c^2)} \tag{13}$$

where, *c* represents the scale parameter of the of the Rayleigh distribution. The CDF of Rayleigh distribution has the following form:

$$F(v_{ins}) = 1 - e^{-v_{ins}^2/(2c^2)} \tag{14}$$

3.3.1.3 Gaussian distribution. The ability of Gaussian distribution to deal with all kind of data, including negative values, and its capability to approximate a large number of natural phenomena has made it a very popular tool in almost all the fields of statistical analysis. The simple and symmetrical bell shaped graphical representation also makes it a visual-friendly tool

to use. Its versatility and familiarity among people has prompted to test its ability to describe ocean current data in the present study. The PDF of a Gaussian distribution can be described as follows:

$$f(v_{ins}) = \frac{1}{\sigma\sqrt{(2\pi)}}\ e^{-(v_{ins}-\mu)^2/(2\sigma^2)} \tag{15}$$

where, μ represents mean velocity while σ represents the standard deviation of the set of data. The CDF of the Gaussian distribution is represented by the following formula:

$$F(v_{ins}) = 0.5 * (1 + \text{erf}(\frac{v_{ins}-\mu}{\sqrt{(2\sigma^2)}}) \tag{16}$$

CHAPTER 4

Assessment

4.1 Velocity Analysis

The time series of the ocean current velocities have been analyzed from HYCOM data at the 16 locations previously described. The results from these computational predictions represent daily-averaged ocean velocities. The depth of the analyzed area is about 3 km. The velocity data do not show much difference within the first 50 meters below the sea level (Figure 4). This fact contrasts with assessments in other regions, e.g., the Florida Straits, where the waters are much shallower and the vertical position makes a stronger difference on the availability of hydrokinetic energy (Duerr & Dhanak, 2012).

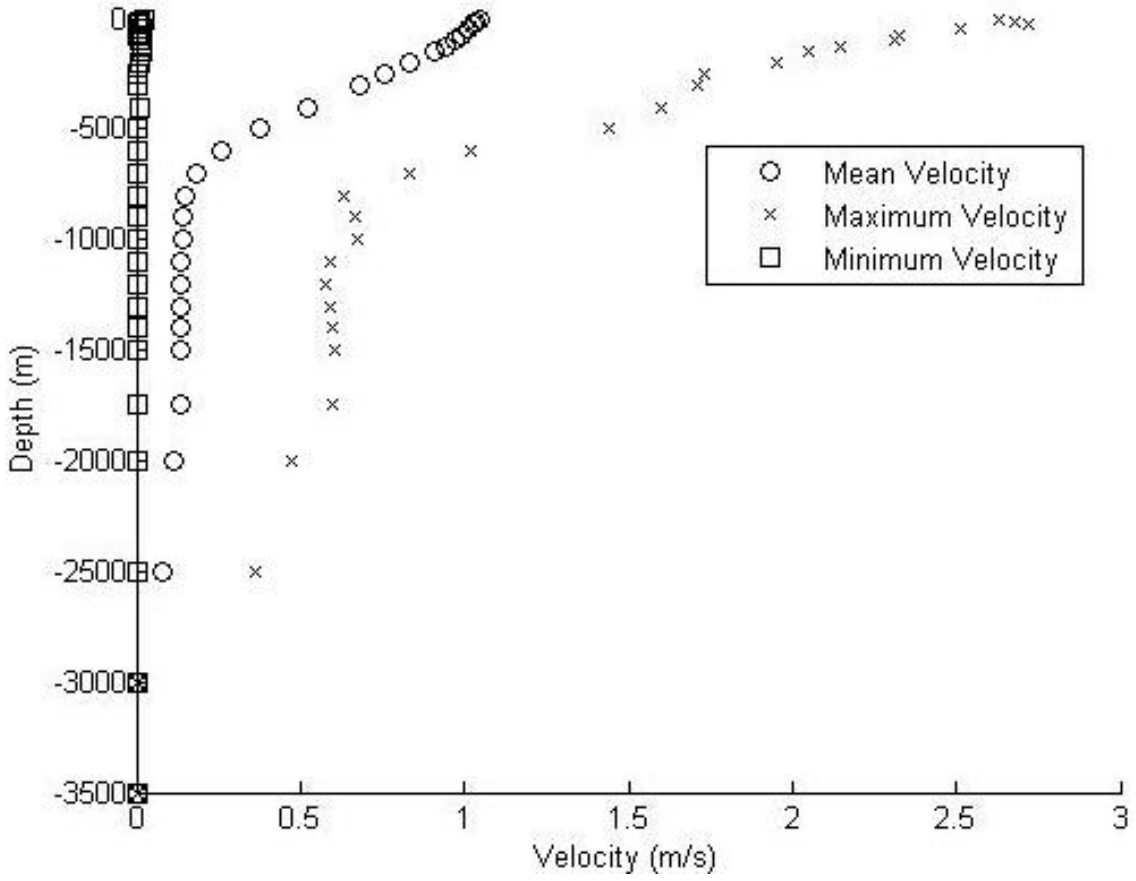

Figure 4. Variation of maximum, minimum, and mean velocity with depth at D1 (HYCOM).

From the qualitative point of view, the 16 locations exhibit a similar temporal evolution and the differences are mainly quantitative. The differences are usually less than 2%. Figure 5 shows the temporal variation for the current velocity at the location A4, B3, C2 and D1 for a depth of 20 m. The temporal variation of the current velocity for the other 12 locations is presented in Appendix A. The median velocity for the almost ten years analyzed is 1.09 m/s for D1.

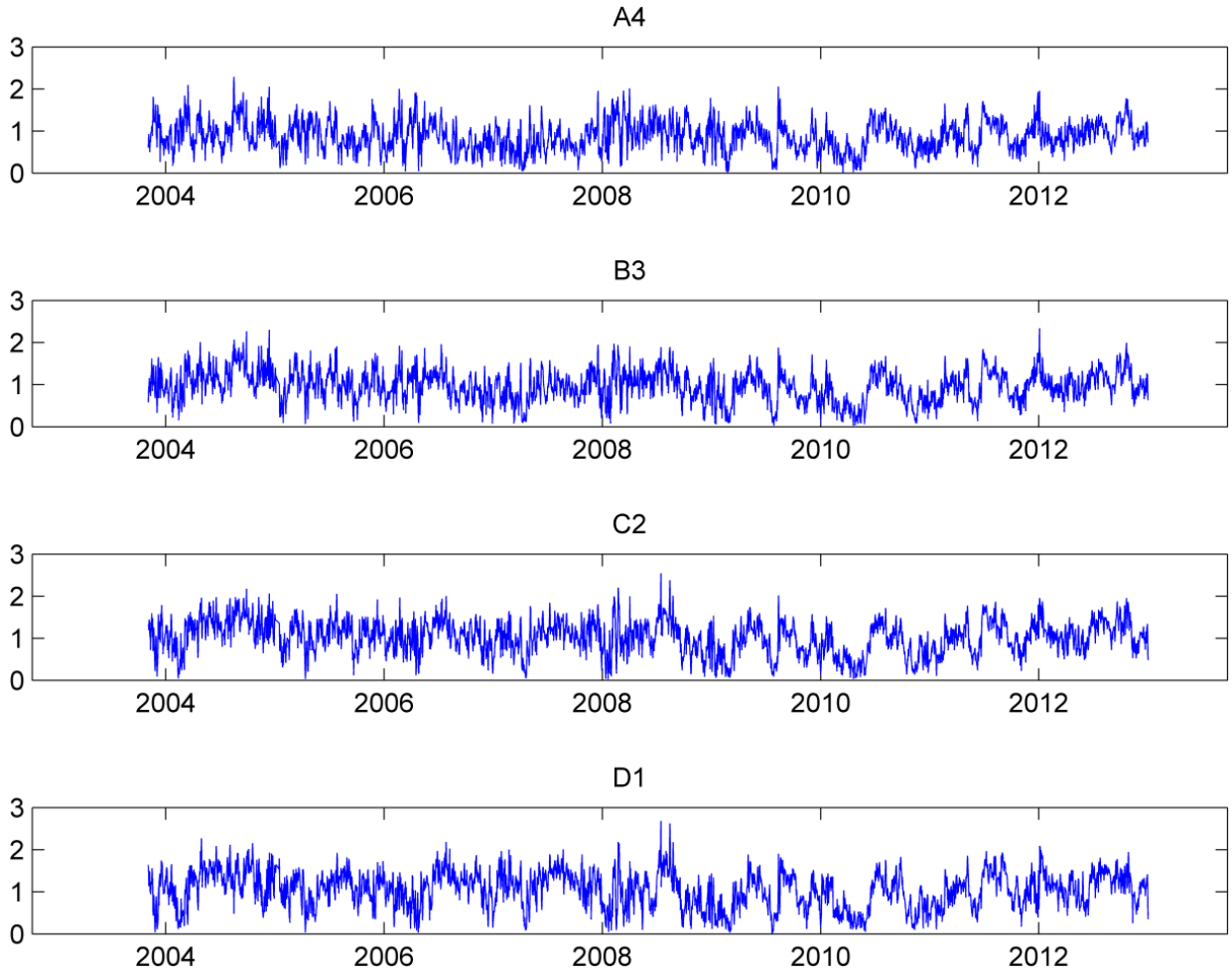

Figure 5. Daily average of ocean current velocity at a depth of 20m at point A4, B3, C2, and D1 between 2004 and 2012 (HYCOM).

An assessment depth of 20m was chosen for the analysis where the maximum velocity reached as high as 2.7m/s computed at C1 and the minimum velocity is practically zero

(0.0077m/s) at B1 in the assessed time period. The temporal mean velocity over the entire period at different positions ranged between 0.87m/s and 1.03 m/s with the maximum mean value recorded at D1, the nearest position of the observed location from the shore. The monthly mean velocity at D1 also shows a seasonal dependency with high velocities recorded during late summer (July-September) whereas low mean velocities are observed during winter (Figure 6).

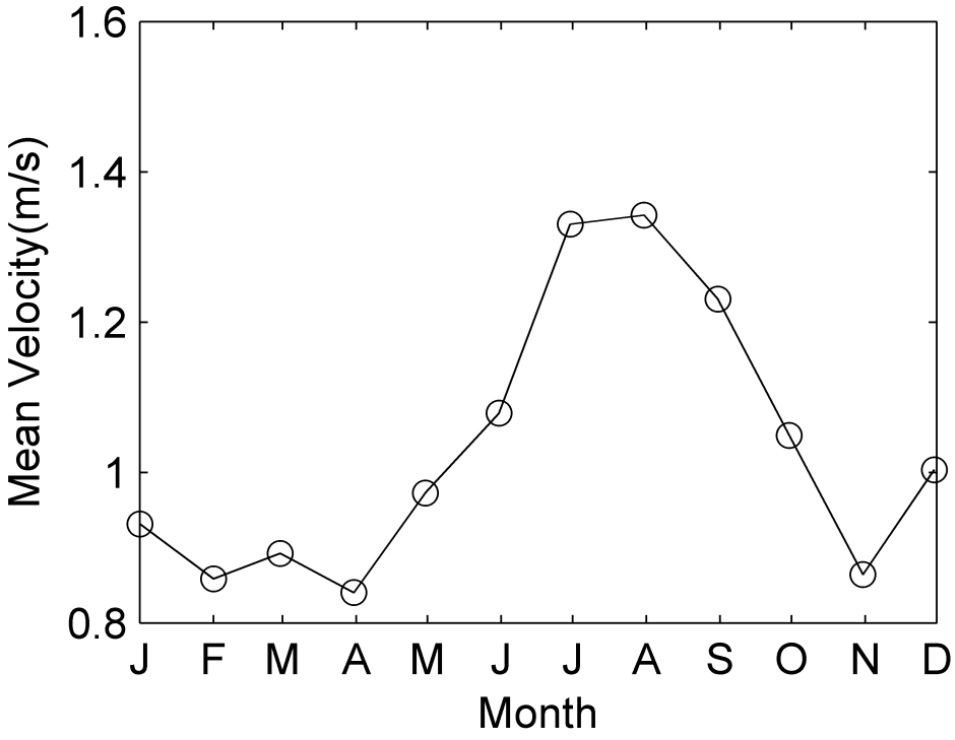

Figure 6. Monthly mean velocity at D1 for the entire period (HYCOM).

The monthly mean velocities for the remaining locations are presented in Appendix A. The medians for the current velocity at the sea surface, and at depths of 20 and 50 m are 1.091 m/s, 1.087 m/s, and 1.073 m/s, respectively at D1. This confirms that depth is not very important in our assessment. Over 80% of the time, the velocity ranges between 0.5 and 1.5 m/s at all the HYCOM locations (Figure 7). The 16 different positions show similar temporal variation with less than 2% variation seen more than 95% of the time.

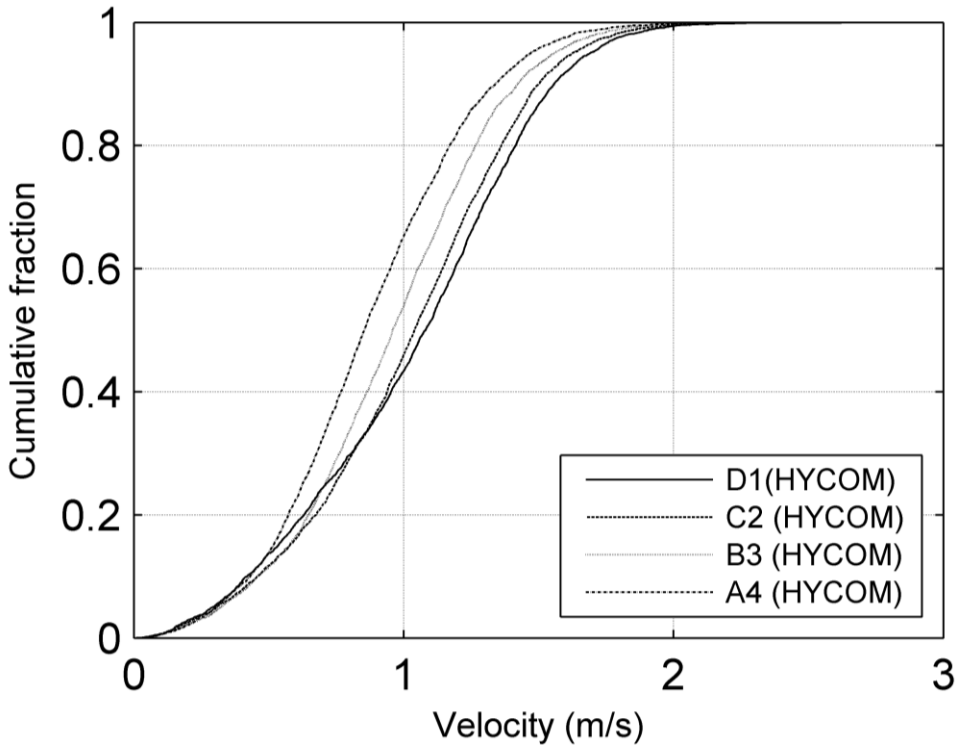

Figure 7. Cumulative distribution of velocities at A4, B3, C2, and D1 for the entire period (HYCOM).

In order to somewhat assess the performance of the numerical predictions, HYCOM data have been compared to measurements taken with a high-frequency radar. The availability of these data is shorter so that the analysis has focused on the 12 months beginning in March 16th of 2012. Some comparisons for the current surface velocity near the location D1 are shown in Figure 8. The radar data have been averaged to get a daily value when several measurements over a period of 24 hours were available. Both sets of data points exhibit similar trends but the predictions from HYCOM exhibit higher velocities than the radar measurements. This reflects in the magnitude for the median velocities, which are 1.09 m/s and 0.81 m/s, respectively.

The HYCOM data and radar measurements are also used to evaluate the preferential direction of the ocean current. Rose plots given as a function of current direction and magnitude are used to visualize these characteristics. Figure 9 shows the rose plots at the radar position

(Figure 9a) and at three locations: A4 (Figure 9b), C2 (Figure 9c), and D1 (Figure 9d) from the HYCOM data. The results indicate that the Gulf Stream flows mostly in the Northeast direction in the studied area. The differences in the current direction between radar and computational data are minimal, although the former exhibits a larger variability. The data also suggest that the further from the center of the Gulf Stream—where the velocity is maximum—the direction of the current is less uniform and areas of recirculation are more likely to be observed.

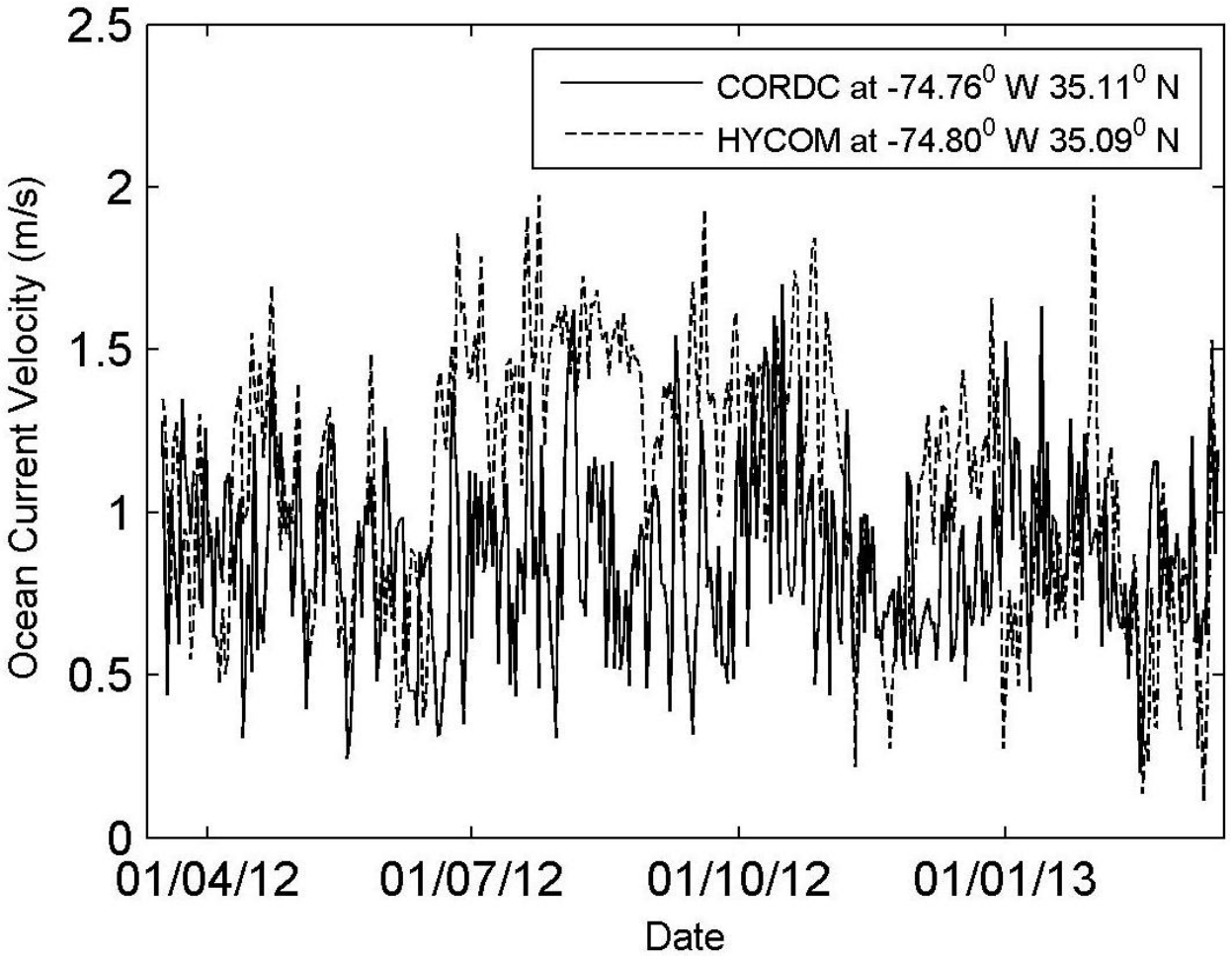

Figure 8. Comparison between HYCOM data and CORDC data.

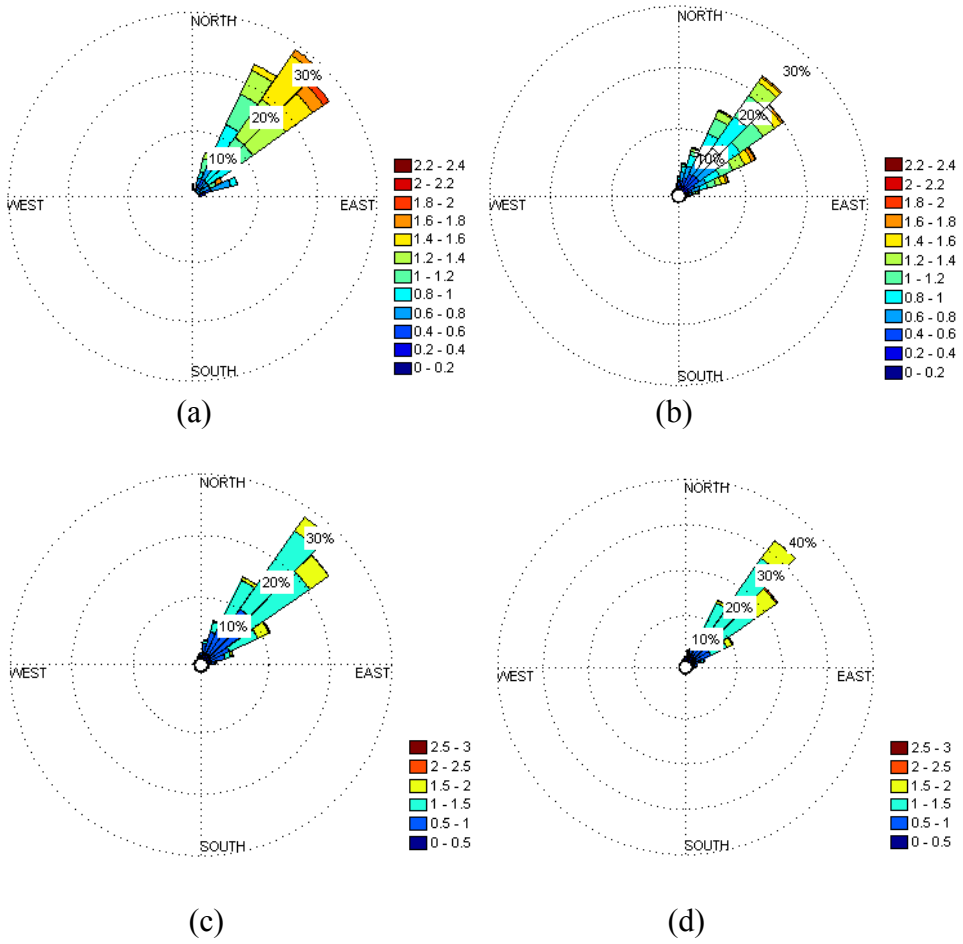

Figure 9. Rose Plots for Ocean Current velocity (a) CORDC measurements, (b) HYCOM data at A4, (c) HYCOM data at C2, (d) HYCOM data at D1.

4.2 Power Density Analysis

The sea water density along the water column of the ocean can be considered to remain constant as the variation is negligible compared to its high value. This makes the power density to be a direct function of the cube of the velocity. A value of 1018 kg/m^3 for sea water density is used for computing power densities in the area of interest. This value corresponds to the density of water for an average salinity of 36.3 PSU (Practical Salinity Unit) and an average temperature of 20°C. About 60% of the time the daily average of power density is between 275W/m^2 and 1200W/m^2 with a peak value of as high as approximately 9800 W/m^2 (Figure 10). The highest

potential for extraction was found to be location 'D1' where over 55% of the days power density is 500 W/m^2 or higher. This reduces to 36% at 'A4.' This can be seen from the cumulative plots of the power densities at 'D1' and 'A4' (Figure 10). The mean power density is also more than 500 W/m^2 for all the 16 different locations with a maximum mean of 856 W/m^2 at location D1 (Table 2).

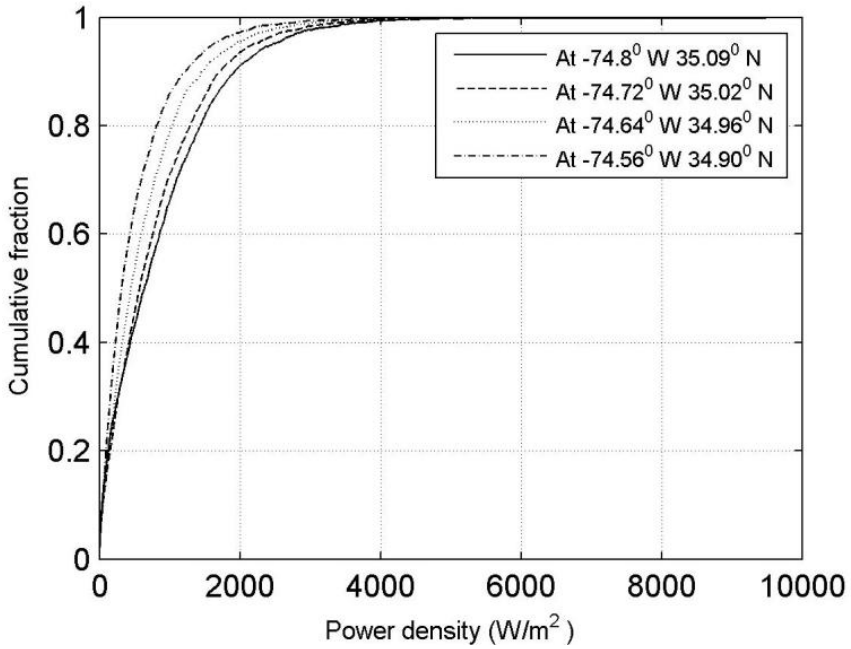

Figure 10. Cumulative distribution of power density from HYCOM data at four different locations.

Table 2

Scale Factor, Shape factor, R^2, Mean Velocity, and Variance for Weibull Fit at Different Locations

Points	Scale Factor, c(m/s)	Shape Factor, K	R^2	Mean Velocity v_{mean} (m/s)	Variance σ^2
A1	1.1152	2.7912	0.9940	.9965	0.1498
A2	1.0773	2.7997	0.9972	0.962	0.1381
A3	1.0309	2.7504	0.9992	0.9193	0.1296

Table 2

(Cont.)

Points	Scale Factor, c(m/s)	Shape Factor, K	R^2	Mean Velocity v_{mean} (m/s)	Variance σ^2
A4	0.9801	2.6504	0.9996	0.8727	0.124
B1	1.1412	2.7643	0.9912	1.0198	0.1596
B2	1.1097	2.8032	0.9946	0.9917	0.1466
B3	1.0703	2.8049	0.9980	0.9555	0.1357
B4	1.0254	2.7474	0.9992	0.9143	0.128
C1	1.1592	2.6982	0.9902	1.0345	0.1722
C2	1.1364	2.7689	0.9934	1.0151	0.1580
C3	1.1021	2.7955	0.9964	0.9847	0.1449
C4	1.0621	2.7779	0.9982	0.9483	0.1348
D1	1.1616	2.5959	0.9882	1.0351	0.1845
D2	1.1517	2.6994	0.9904	1.028	0.1694
D3	1.1296	2.7646	0.9944	1.0092	0.1556
D4	1.0972	2.7822	0.9970	0.9804	0.1441

4.3 Statistical Analysis

Once the time series for each location had been analyzed, statistical tools were introduced to evaluate their applicability. More specifically, the discrete data from HYCOM were modeled using PDFs. Among the PDFs, the Rayleigh, Gaussian, and Weibull distributions have been used for the assessment process. The latter PDF requires estimating the shape and scale factors, which is accomplished using the MLE method. The analysis was performed over the 16 aforementioned locations. All of them exhibited similar trends and among them four locations have been selected (A4, B3, C2, and D1) to illustrate the findings. Figure 11 shows the velocity

histogram and the calculated probability density functions at the selected locations. The probability plots of the remaining locations are presented in Appendix B.

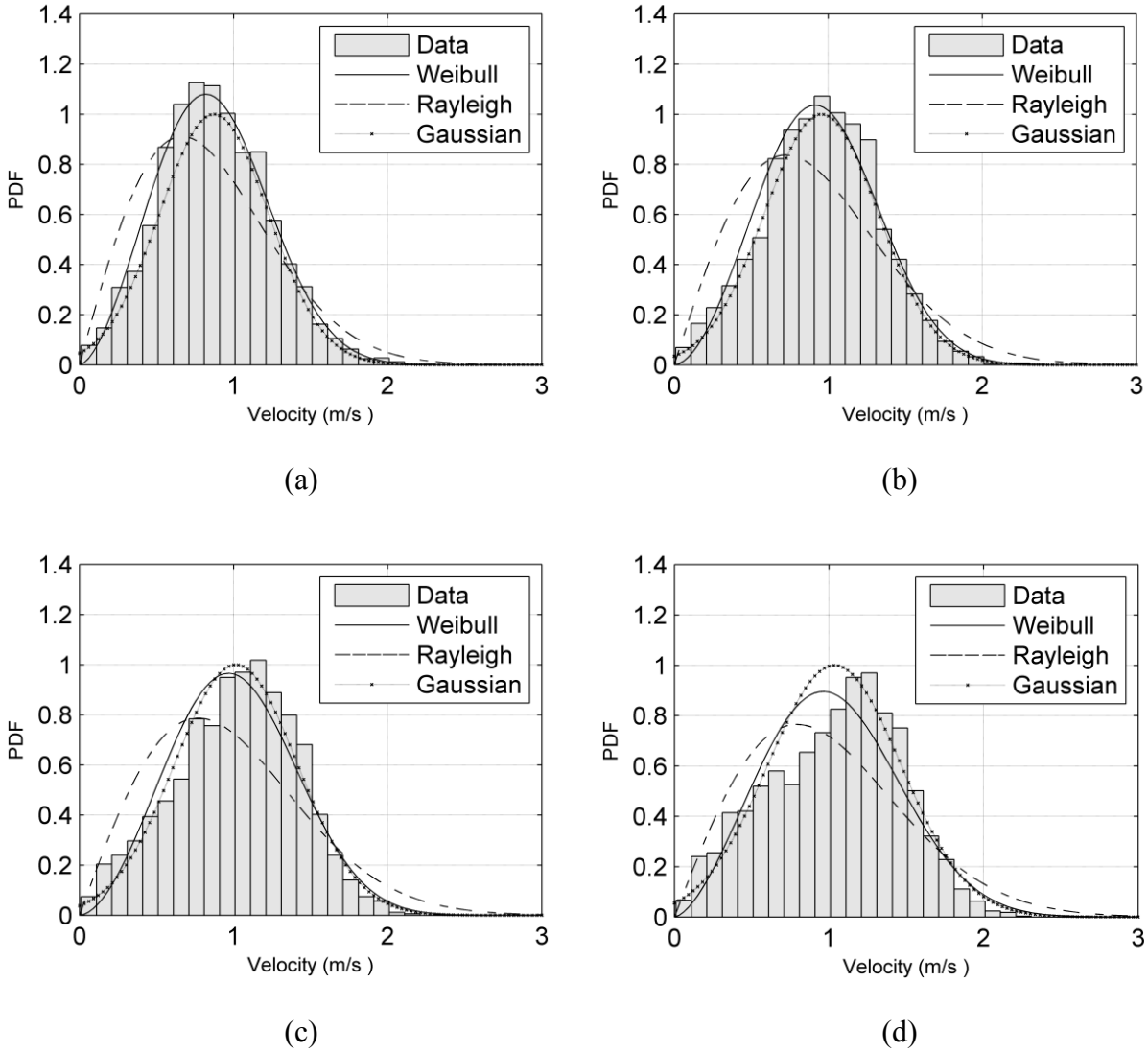

Figure 11. Ocean current velocity histogram and predictions from the probability density functions at four different locations (a) A4; (b) B3; (c) C2; (d) D1.

The velocity histograms show that the most likely velocity is around 1 m/s for all the locations. However, there is a higher likelihood of observing velocities greater than 1.0 m/s and close to 2.0 m/s at D1 than at A4. This is reflected in the magnitude of the Weibull scale parameter, shown in Table 2, which progressively increases for A4, B3, C2, and D1. The shape

factors for these locations range between 2.596 and 2.805, which suggests a slight skewing of the velocity series but not as large as a Rayleigh distribution would indicate. Visual inspection suggests that the Weibull distribution is the better predictor. A root-mean-squared-error (RMSE) analysis on the three PDFs has also been conducted. A summary of the error analysis is also shown in Table 3. It corroborates that the Weibull distribution is the most accurate of the three. All the medians predicted by the Weibull distribution fall within 5% of the margin of error when compared to the raw data.

Table 3

Evaluation of RMSE for Weibull, Rayleigh, and Gaussian Distributions at Locations A, B3, C2, and D1

Position	Weibull Shape Parameter	Weibull RMSE	Rayleigh RMSE	Gaussian RMSE
A4	2.6504	0.7693	0.8041	0.7698
B3	2.8049	0.7856	0.8314	0.7820
C2	2.7689	0.7736	0.8138	0.7673
D1	2.5959	0.7684	0.7909	0.7607

The raw data and Weibull distributions are used to evaluate the power density for the Gulf Stream in the area of interest. Although the data from HYCOM are not instantaneous values but daily averages, we have used equation 2 to estimate power density. This provides a conservative estimate but we have preferred this option over the use of the daily variance as an estimate of the variance of the stream velocity, which would introduce another source of uncertainty. The cumulative power density is shown in Figure 12. The predictions from the Weibull model lay very close to the raw data. For example, the discrepancy at location D1 is less than 1% for the cumulative distribution function. The location D1 is the one with the

highest potential from an energy point-of-view as the results suggest that, for example, over 55% of the days will see a power density of 500 W/m^2 higher. This percentage decreases to 35% at the location A4.

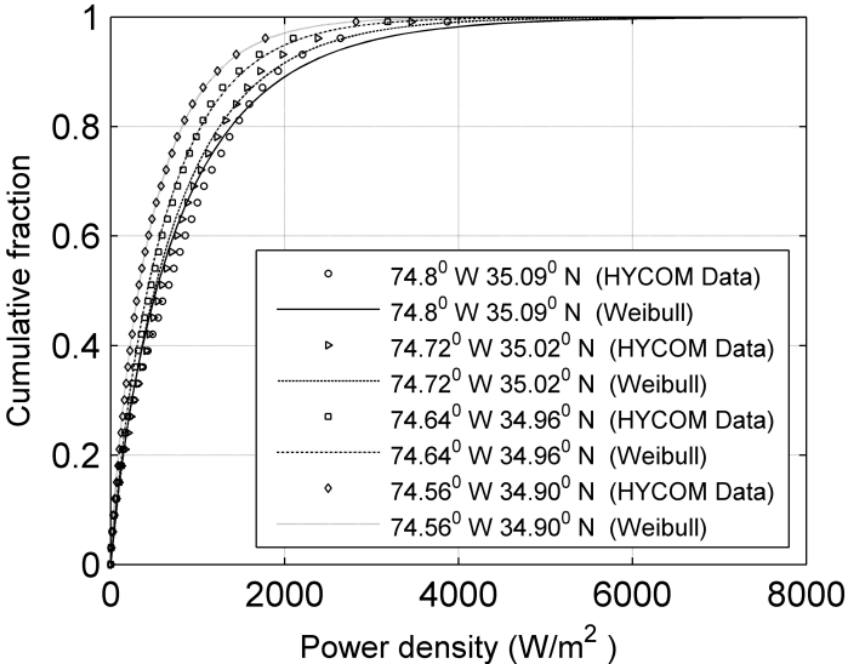

Figure 12. Comparative cumulative distribution of power density from HYCOM data and Weibull.

In order to assess the error arising from the use of PDFs, the discrepancy between the raw data and the predictions from the Weibull and Gaussian distributions for the cumulative distribution of power density have been evaluated. Figure 13(a) and 13(b) show these errors in percentage, for the Weibull and Gaussian distributions, respectively. Although the Gaussian distribution was able to reproduce the velocity statistics similar to the Weibull distribution, it does a weaker job in the prediction of power density. This is partially explained because the Gaussian distribution possesses negative velocities, which do not contribute to power density.

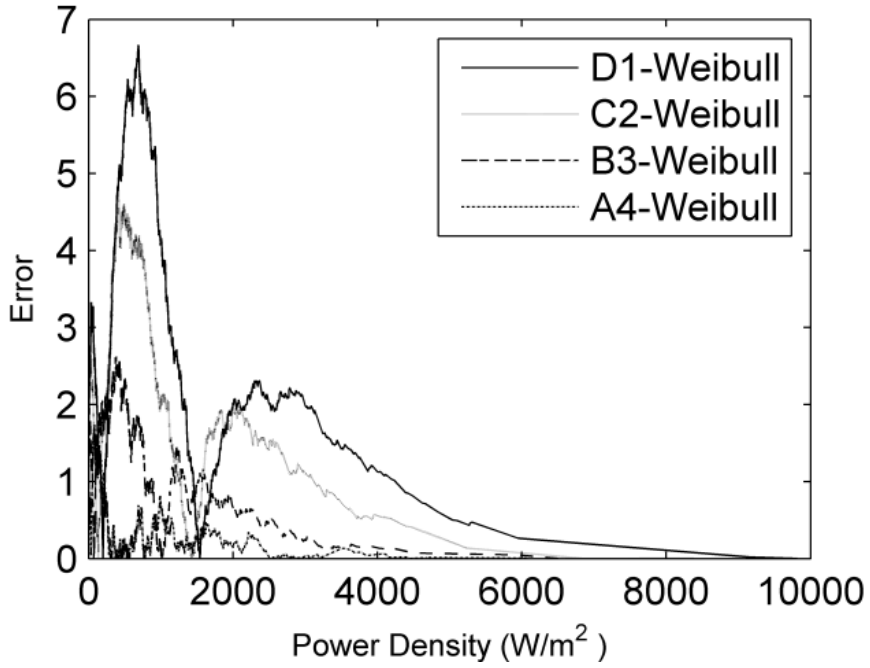

(a)

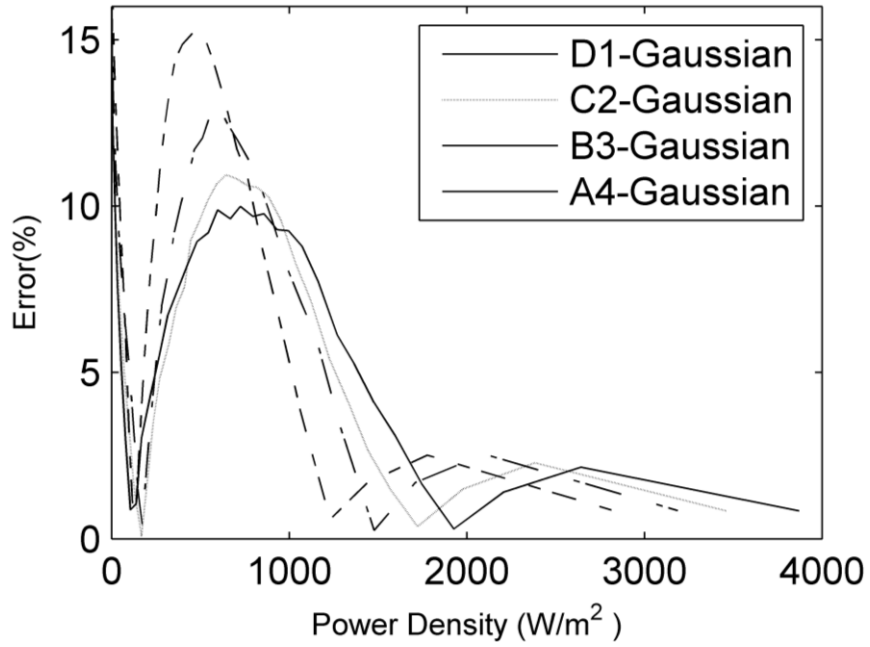

(b)

Figure 13. Error between the Raw data and the prediction from the PDFs for the cumulative distribution function of the power density: (a) Weibull distribution; (b) Gaussian Distribution.

Similar analyses were conducted in the aforementioned regions for one year of data. The results from 2012 data are listed in Table 4 shows that the PDFs are very well described by the Weibull and Gaussian distribution whereas the Rayleigh distribution proves to be a much weaker tool for this purpose. Visual inspections of the PDF plots (Figure 14) also agree with the analysis.

Table 4

Evaluation of RMSE for Weibull, Rayleigh and Gaussian distributions at locations A, B3, C2 and D1 for 2012

Position	Weibull Scale Parameter	Weibull Shape Parameter	Weibull RMSE	Rayleigh RMSE	Gaussian RMSE
A4	1.0584	3.8222	1.0977	1.4724	1.0788
B3	1.1713	3.7773	1.0892	1.4338	1.0705
C2	1.2562	4.0022	1.0257	1.3598	1.0269
D1	1.2826	3.9654	1.0585	1.3912	1.068

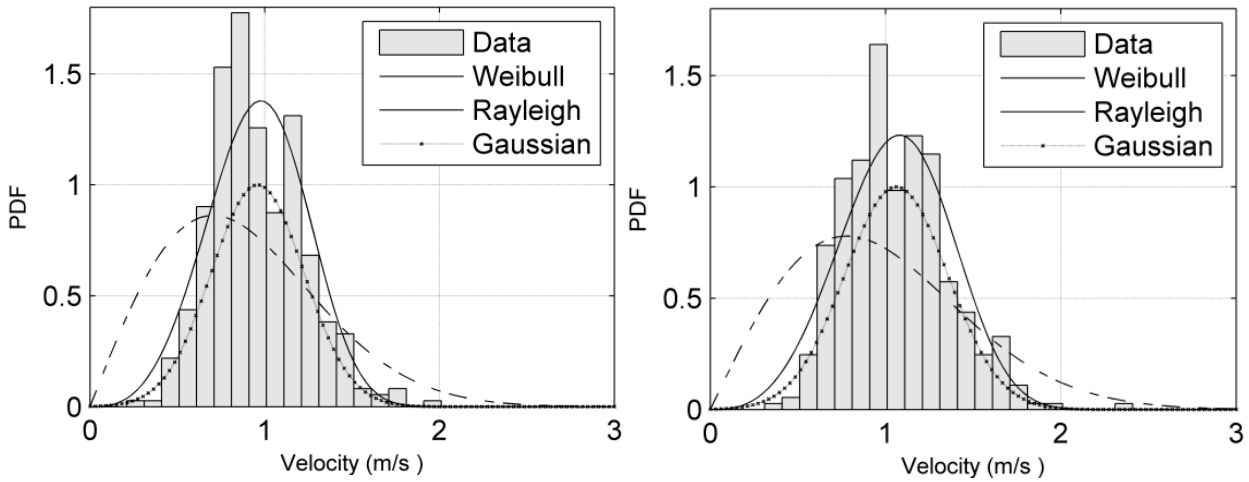

(a) (b)

Figure 14. Ocean current velocity histogram and predictions from the probability density functions at four different locations (a) A4; (b) B3; (c) C2; (d) D1 for the year 2012.

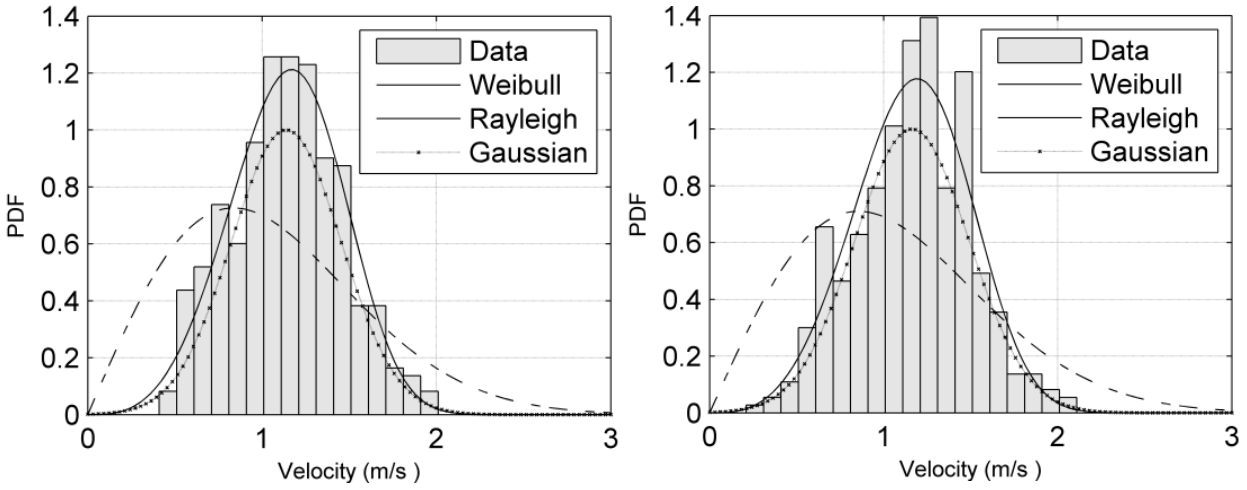

(c) (d)

Figure 14. (Cont.)

4.4 Location of Optimal Position for Energy Extraction

In a given region, different locations may have different characteristics for extraction of energy. These characteristics will have direct impact on the economic viability of energy extraction from these locations. So an analysis for determining the optimal position for energy extraction will not only reduce the efforts of site inspections but also be economically feasible.

The selection of an optimal position for extracting power depends primarily on two types of factors. Even though the energy potential of the location is the most important aspect for selecting a location, the characteristic of the site also has its own importance. The primary factor which determines the energy potential in a given location is power density of that region. If the site does not produce sufficient energy to be extracted, the other factors lose their importance. Moreover, with the increase in available power density the economic feasibility of energy extraction increases.

The geographical characteristics of the location of assessment have its influence the economic feasibility of energy extraction. As the location gets further away from the shore, the

cost of extraction of energy from the potential site increases due to the increased distance for energy transmission. This will also result in increase in maintenance cost, as the team has to travel deeper into the ocean. The increase depth of the seafloor at the site also increases the installation and maintenance cost as it will require a more complex mooring system for the extraction device. Duerr (Smentek-Duerr, 2012) proposed an expression of a term named location factor (LF) to locate the optimum position for energy extraction where each of the factors are temporarily averaged and normalized by the maximum available value. This is given as follows:

$$LF = \alpha \times a + \beta \times b - \lambda \times c - \eta \times d \,, \tag{13}$$

where 'a' is the normalized power, 'b' is the normalized area containing power density above a threshold value (0.5kW/m^2), 'c' is the normalized distance from the shore, and 'd' is normalized depth of the sea floor bed, while α, β, λ, and η represents the weighing factor of the respective variables to determine importance of these factors. The position bearing the maximum value of location factor is considered the most optimum position among the available points.

But for smooth power generation from a specific site using a hydrokinetic device, the importance of flow direction of the ocean current cannot be neglected. It has a direct impact on the fraction of available power that can be extracted. The less there is fluctuation in the direction of ocean current, the more there is stability in the flow, requiring less change in the direction the energy extraction device is facing. As this assessment mainly concerns with energy extraction at a specific depth, the first two factors 'a' and 'b' can be considered to have similar effect for extraction of energy. So these two factors are replaced by a factor 'a,' which is the normalized power density in the location of interest. A new term 'e' is introduced into the expression the effects of fluctuation in flow direction. This new variable 'e' is the normalized standard

deviation of the direction of flow and ε is its weighing factor. The new expression gets the following form:

$$LF = \alpha \times a - \varepsilon \times e - \lambda \times c - \eta \times d \,, \tag{14}$$

where

$$a = \frac{P}{P_{\max}} = \text{normalized mean power density} \tag{15}$$

$$e = \frac{\omega}{\omega_{\max}} = \text{normalized flow direction variation} \tag{16}$$

$$c = \frac{L}{L_{\max}} = \text{normalized minimum distance from shore} \tag{17}$$

$$d = \frac{D}{D_{\max}} = \text{normalized sea-floor depth} \tag{18}$$

ω = difference between upper and lower limit of 95% confidence interval of flow direction

$\alpha, \varepsilon, \lambda, \eta$ = weighing factor for a, e, c, d

The analysis was conducted throughout the site considering all weighing factors equal to unity. Almost all of the locations had similar maximum depths of about 3 km except for locations A3 and A4. These two locations which are also the farthest and third farthest locations from the shore have a maximum depth of around 3.5 km. Strong power potential is observed near location D1, also the nearest point from the shore, with the potential gradually decreasing in the south eastern direction. The flow direction fluctuation in all the assessed locations were almost of similar value with high variation located near D2 and low variation was observed at B3.

Based on the current analysis the most optimum location for extraction of power was located at D1, which also has the maximum power potential. The results of the analysis are tabulated in Table 5.

Table 5

Parameters for Computing Location Factor

	Distance, km	Depth, m	Power Density, W/m^2	Angle Standard Deviation, degree	Location factor, LF
A1	76.6	3000	731.5851	27.0577	-1.773
A2	82.91	3000	655.9664	26.0961	-1.8925
A3	89.37	3500	577.3237	26.5648	-2.2114
A4	95.95	3500	503.4868	27.1675	-2.3879
B1	73.07	3000	788.4891	26.8172	-1.6611
B2	79.65	3000	718.5544	26.7172	-1.8078
B3	86.35	3000	642.031	25.5112	-1.9236
B4	93.14	3000	567.8073	25.5945	-2.0841
C1	70.12	3000	835.5576	26.58	-1.5669
C2	76.95	3000	777.2153	26.7675	-1.7129
C3	83.86	3000	703.8844	26.5689	-1.8634
C4	90.83	3000	629.3421	25.5878	-1.9879
D1	67.83	3000	856.195	26.4383	-1.5138
D2	74.87	3000	818.8914	27.8381	-1.681
D3	81.95	3000	762.9821	27.6517	-1.8134
D4	89.06	3000	695.3186	26.9436	-1.9411

4.5 Global Assessment

There are five major ocean gyres in the world's oceans. Depending on the location, each of these gyres consists of two parts; the narrow, deep western boundary current and the broad, shallow eastern boundary current. The western boundary currents are comparatively much stronger and fast moving and can be considered future prospects of harnessing ocean current energy. The locations of these fast moving western moving currents were analyzed using one year's data from 2012. Six regions were located with a prospect of harnessing ocean current energy. These regions are the Agulhas current (south) near the coast of South Africa, the Agulhas current (north) near Somalia, the North Equatorial current near Indonesia, the Kuroshio current in the southeast coast of Japan, the North Brazil current, and the Mozambique current on the east coast of Madagascar.

Once the initial sites are chosen, each of the regions are analyzed based on the mean velocity of the entire 2012 at the assessment depth. This allowed the selection of a fixed location on each of the regions with the highest mean velocity throughout the year. Plots showing distribution of mean velocities in four of the regions are shown in Figure 15. Once the specific locations are chosen at each of the assessment site, all the PDFs are applied on those locations to assess their applicability in the world's oceans.

The results of this analysis conducted at the same assessment depth as the Gulf Stream are summarized in Tables 6 and 7. Once the power density is considered as the scale for assessment, it has been observed that the South Agulhas current in South Africa has the maximum potential region with a mean power density more than $2kW/m^2$ for the year 2012. The Kuroshio current near Japan also had a power density close to the 2kW/m2 mark followed by the

Agulhas current near Somalia and the Mozambique current with both having power density more than 1200 W/m^2.

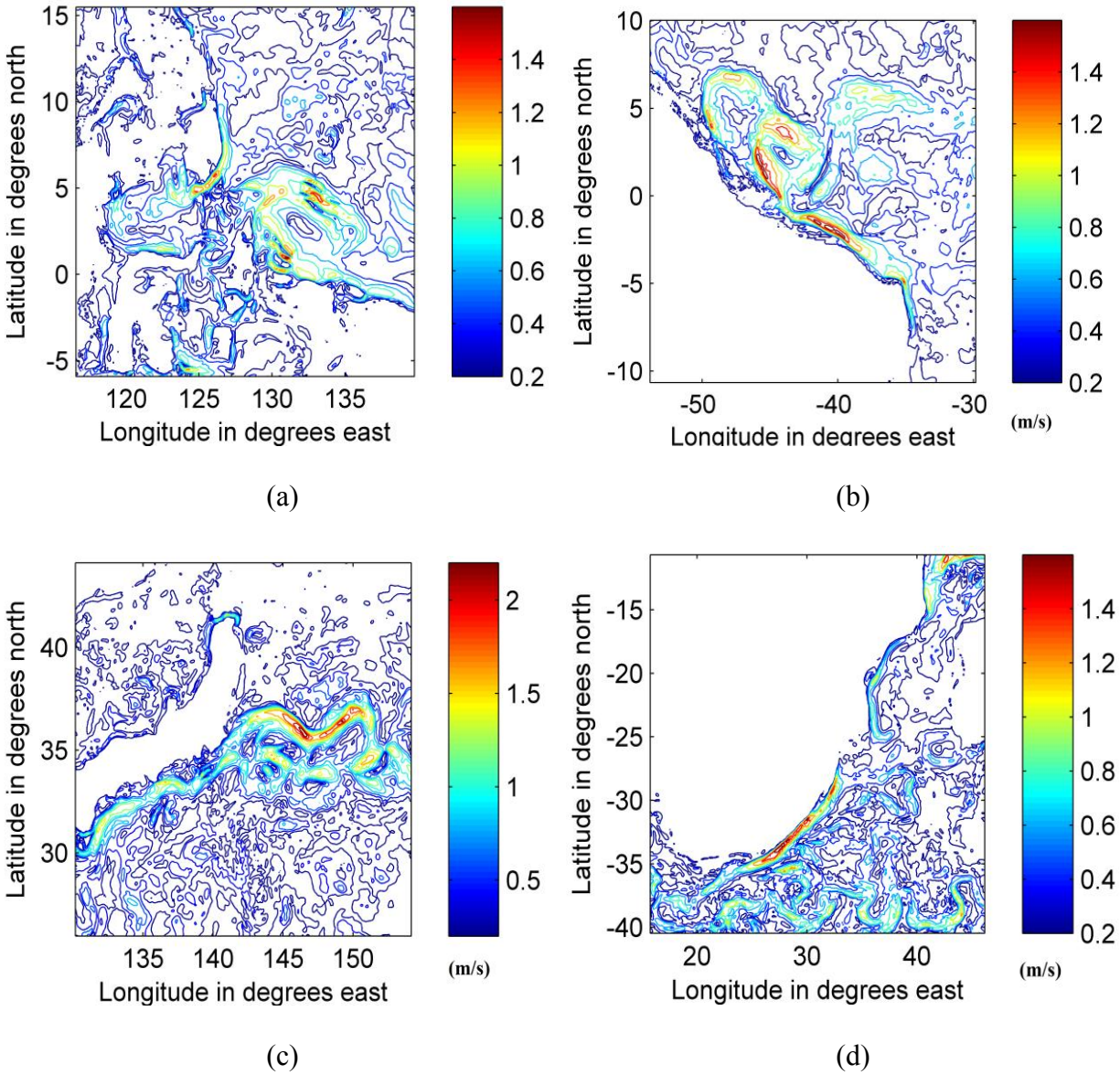

Figure 15. Regions with high potential of ocean current energy in terms of mean velocity of 2012 at different locations of world ocean (a) North Equatorial Current, (b) North Brazil Current, (c) Kuroshio Current in Japan and (d) Agulhas current in South Africa.

Table 6

Assessment and Location Parameters at Different Ocean Gyres of the World in 2012

	Latitude degrees north	Longitude degrees east	Shape Parameter, k	Scale Parameter, c	Power Density, W/m^2
South Africa	-34.0403	27.04	4.397	1.6608	2115.30
Japan	36.0056	145.84	2.965	1.5388	1867.80
Somalia	4.2361	48.24	1.7529	1.2068	1397.50
Madagascar	-11.9915	49.4399	3.5695	1.3823	1269.90
Brazil	0.72	-44.8	2.414	1.04	647.3822
Indonesia	0.96	131.04	2.6712	1.0281	586.6735

Table 7

RMSE and r2 Regarding Fitting of PDFs at Different Locations

	Weibull r^2	Rayleigh r^2	Gaussian r^2	Weibull RMSE	Rayleigh RMSE	Gaussian RMSE
South Africa	0.9908	0.9158	0.9851	1.0797	1.4007	1.107
Japan	0.9853	0.9359	0.9914	1.1058	1.2394	1.0844
Somalia	0.9954	0.9922	0.9841	1.0215	1.0527	1.0773
Madagascar	0.9561	0.8703	0.9545	1.1816	1.4368	1.189
Brazil	0.9805	0.9573	0.9934	1.1053	1.1823	1.0432
Indonesia	0.9916	0.9631	0.9966	1.0338	1.1545	1.0024

The analyses of PDFs are applied in these regions to observe their applicability in other ocean gyres. The r^2 and the RMSE value of the PDFs, tabulated in Table 7, compared to the model velocity data in those locations, suggests similar results as achieved in the study of the Gulf Stream. The Weibull and Gaussian distributions proved to be a better predictor of ocean current gyres compared to the Rayleigh distribution for all the locations that have been

examined. It can also be observed from velocity histograms combined with the PDF plots of these three tools for the analyzed location (Figure 16).

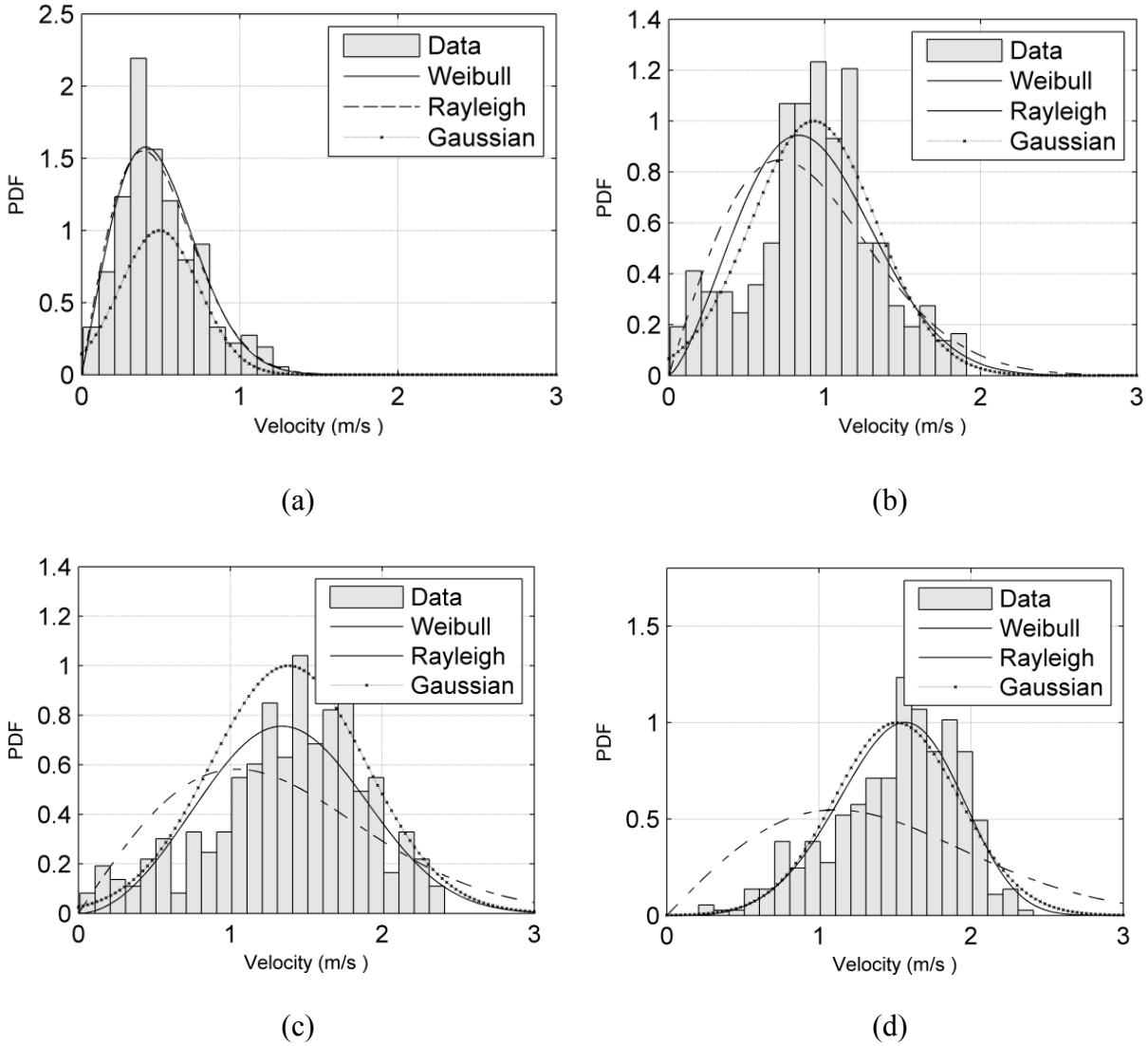

Figure 16. PDF plots at (a) North Equatorial Current in Indonesia, (b) North Brazil Current, (c) Kuroshio Current in Japan, (d) Agulhas current in South Africa.

4.6 Tidal Energy Assessment near Cape Hatteras

Although tidal current energy is not similar to ocean current in terms of the continuity of flow, with the flow changing phase 2 or 4 times a day, the dynamics it follows at each phase is

similar. This has prompted the attempt of a similar approach in this field with a view to use the results as an initial step for future studies.

The first step in this process was to select a location to conduct the analysis. This was facilitated by a report on tidal energy potential throughout the United States prepared by the Georgia Tech Research corporation (Haas, 2011). One of the sites with good potential in North Carolina indicated by the report was the Ocracoke inlet near Cape Hatteras (Figure 17). This site was chosen as the assessment site to conduct the analysis.

Figure 17. Geographical location of the area of interest for tidal energy assessment. Source: http://www.tide-forecast.com/locations/Ocracoke-Inlet-North-Carolina

As some of the tidal constituents governing the tidal cycle have a period less than one day, the daily average velocity data from HYCOM are incapable of presenting the tidal characteristics of a certain location. So a different model was required for the tidal analysis. The Regional Ocean Modeling System (ROMS), a free-surface, terrain-following, primitive equations ocean model (Haidvogel et al., 2000) with a temporal resolution of hourly averages has been selected for the current study. A total of one year's data was used spanning between May 18th, 2013 and May 17th, 2014.

The first step in the analysis was to calculate the number neap tides and spring tides in a tidal cycle (usually 29 days; Haas, 2011) to ensure that tidal cycle exists in the area of assessment. The overall velocity distribution for the month of August in 2013 shown in Figure 18(a) shows that each month contains two spring tides and two neap tides. The ebb and flood directions are shown in Figure 18(b). The direction-wise (positive indicating flood and negative indicating ebb) time-series plot of the velocities (Figure 19) shows that the velocity values during a day do not differ much between the flood and the ebb.

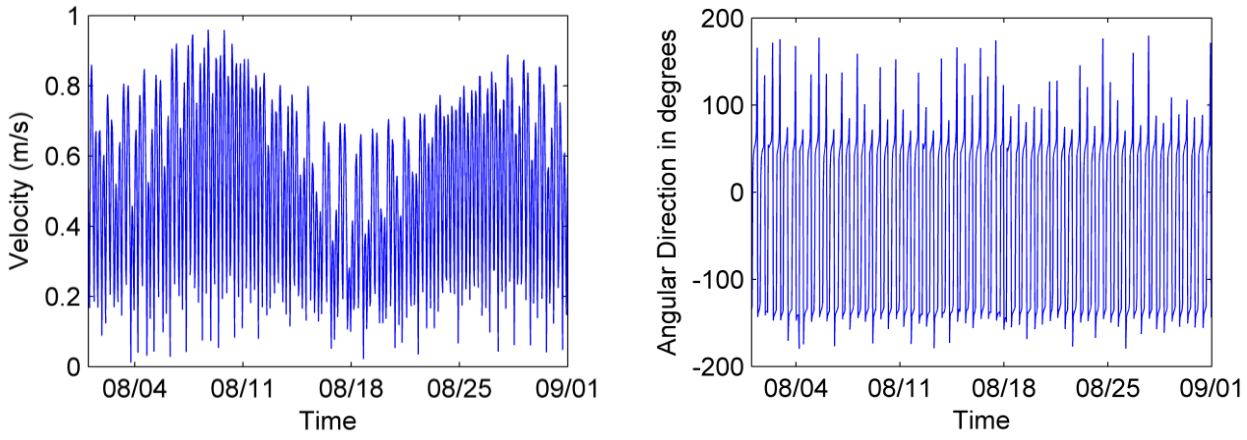

(a) (b)

Figure 18. Overall (a) velocity distribution and (b) directional distribution of tidal current for the month of August.

In the next step, the three PDFs are applied for the entire years of data for all the three cases (overall, flood, and ebb) to evaluate their applicability in the field of tidal energy. The results of this analysis are presented in Table 8.

Results similar to ocean current energy was observed for the overall tidal current flow with Weibull and Gaussian being superior to Rayleigh in capturing the properties. Between themselves, the Weibull was a slightly better predictor for the overall flow while the Gaussian

predicted the flood flow well. But the Weibull was far more superior in capturing the properties of the ebb flow. The PDF plots (Figure 20) also show similar results for all three types of flows.

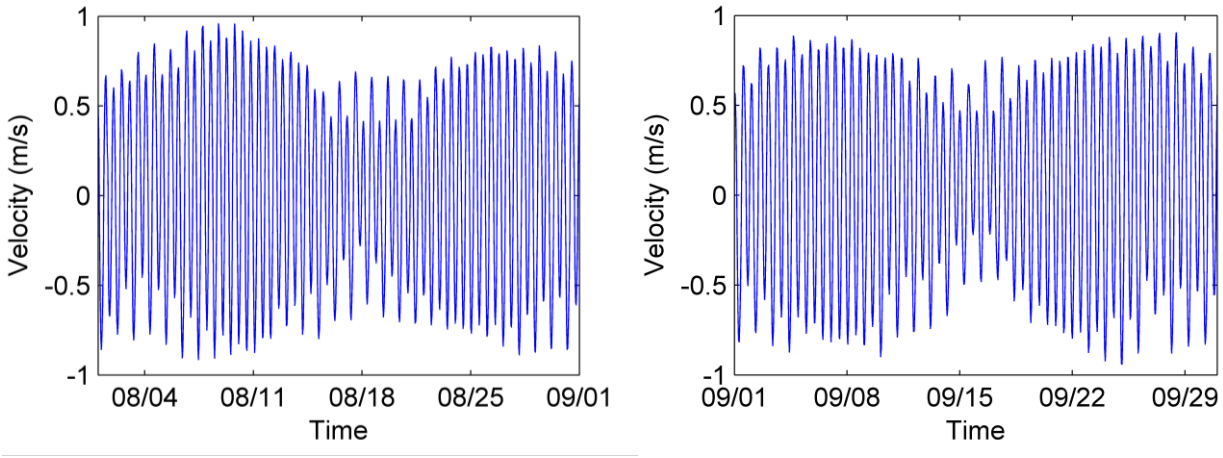

(a) (b)

Figure 19. Velocity Distribution with phase change at the site during (a) August; (b) September.

Table 8

RMSE and r2 Regarding Fitting of PDFs at Different Flows

Region	Primary Location	Flow type	Scale Parameter c	Shape Parameter, k	Power Density W/m^2	Weibull RMSE	Rayleigh RMSE	Gaussian RMSE
Cape-Hatteras	Ocracoke inlet	Overall	0.8867	2.2145	429.0858	1.0087	1.0239	1.0139
		Flood	0.8991	2.3663	424.3166	1.1043	1.1075	1.0967
		Ebb	0.875	2.0867	435.1272	1.0831	1.0836	1.2967

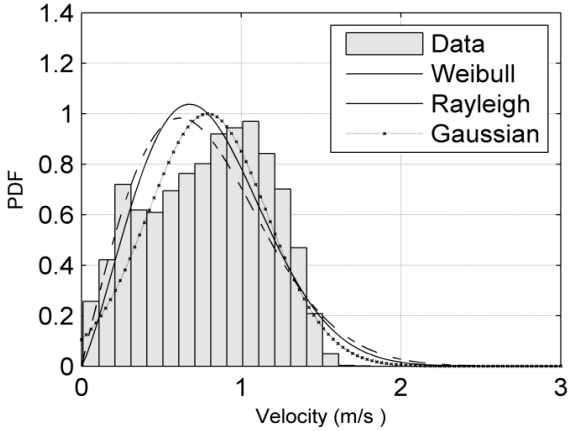

(a)

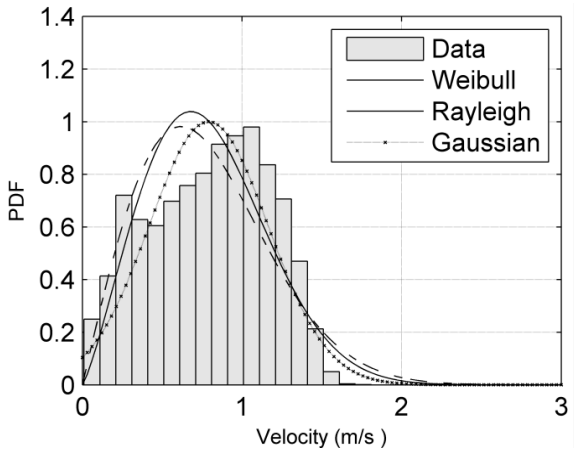

(b)

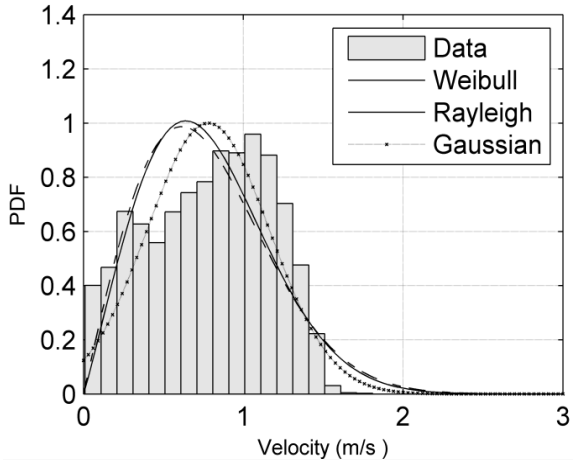

(c)

Figure 20. PDF plots of tidal current for (a) overall flow, (b) flood, (c) ebb.

CHAPTER 5

Discussion and Future Research

The Gulf Stream's location in the vicinity of the U.S. Atlantic coast has resulted in an increased interest in its study as a potential source of renewable energy. The increased transport of the current near Cape Hatteras, North Carolina, has motivated the completion of a detailed assessment of available hydrokinetic energy. The research described in this dissertation analyzes the prospect of harnessing energy from the Gulf Stream near Cape Hatteras, and it introduces probability density tools as a means to analyze the available energy from ocean currents.

The assessment was conducted in an area covering approximately 482.67 km^2, about 65 km east from Cape Hatteras. The analysis has been conducted using long-term data from HYCOM in addition to available high frequency radar measurements from CORDC. The latter data contained hourly averages but covered only 12 months. Both sources of data are known to include uncertainty and, therefore, developments in computations and ocean current measurements should result in future refinements of the present and similar assessments. The assessment has shown good potential for energy extraction in the area of study with at least 36% of the time power density exceeding 500 W/m^2. The northwest corner in the studied area has been identified with highest potential as it exhibits power density 275 W/m^2 or higher over 70% of the days. Low directional variability of the stream is also observed in this region, which contrasts with wind energy where high fluctuations in wind direction are very common. Our study has also shown some seasonal dependency of the flow but negligible difference along the upper portion of the water column.

The study has also explored the utilization of the Weibull, Rayleigh, and Gaussian distributions to describe current velocities and power densities. Among these distributions, the Weibull and Gaussian distributions are able to capture the main statistical characteristics of the ocean velocity. However, unlike for a Gaussian distribution, the lack of negative values from the predicitions by a Weibull distribution resulted in a more accurate prediction for power density. Therefore, the use of a Weibull function is recommended for future assessment of hydrokinetic energy from ocean currents. The analysis also provided similar results when applied to other ocean gyres.

The methodology presented here, although in a small scale, has also been used to study the applicability of probability density functions in the field of tidal energy near the shores of North Carolina. The Weibull distribution also results in more accurate predictions than the Rayleigh or Gaussian distributions. However, this study has been conducted only for one location and needs to be conducted at other locations with different latitudinal values. In addition to the findings presented here, there still remain places for improvement in the assessment of ocean current energy. The HYCOM data used for the analysis are daily averages which do not have sufficient resolution to indicate any information regarding the effects of different constituents throughout a day. The availability of finer data should increase the reliability of the predictions. Other factors, such as environmental impact or socio-economic considerations, will become important as this technology becomes a piece of the renewable energy puzzle.

References

BP. (2013). *BP Statistical Review of World Energy 2013,* p.l.c.

Celik, A. N. (2004). A statistical analysis of wind power density based on the Weibull and Rayleigh models at the southern region of Turkey. *Renewable Energy, 29*(4), 593–604.

Chassignet, E. P., Hurlburt, H. E., Smedstad, O. M., Halliwell, G. R., Hogan, P. J., Wallcraft, A. J., . . . Bleck, R. (2007). The HYCOM (hybrid coordinate ocean model) data assimilative system. *Journal of Marine Systems, 65*(1), 60–83.

Coastal Observing Research and Development Center. (2014). *About CORDC.* Retrieved from http://cordc.ucsd.edu/about/about.php

Costa Rocha, P. A., de Sousa, R. C., de Andrade, C. F., & da Silva, M. E. V. (2012). Comparison of seven numerical methods for determining Weibull parameters for wind energy generation in the northeast region of Brazil. *Applied Energy, 89*(1), 395-400.

Center for Climate and Energy Solutions. (2014, January). *California cap-and-trade program summary.*

Duerr, A. E., & Dhanak, M. R. (2012). An Assessment of the Hydrokinetic Energy Resource of the Florida Current. *IEEE Journal of Oceanic Engineering, 37*(2), 281–293.

Energy Information Administration. (2014). China Overview—U.S. Energy Information Administration, U.S. Energy Information Administration.

Energy Information Administration. (2012). *Annual Energy Outlook 2012.*

Esteban, M., & Leary, D. (2012). Current developments and future prospects of offshore wind and ocean energy. *Applied Energy, 90*(1), 128–136.

Garcia, A., Torres, J. L., Prieto, E., & de Francisco, A. (1998). Fitting wind speed distributions: A case study. *Solar Energy, 62*(2), 139–144.

Haas, K. A. (2011). *Assessment of energy production potential from tidal streams in the United States.* Georgia Tech Research Corporation.

Haidvogel, D. B., Arango, H. G., Hedstrom, K., Beckmann, A., Malanotte-Rizzoli, P., & Shchepetkin, A. F. (2000). Model evaluation experiments in the North Atlantic Basin: simulations in nonlinear terrain-following coordinates. *Dynamics of Atmospheres and Oceans, 32*(3), 239–281.

Halliwell, G. (2002). *HYCOM overview.* Retrieved from http://hycom.org/attachments/067_overview.pdf

Hennessey Jr., J. P. (1977). Some aspects of wind power statistics. *Journal of Applied Meteorology, 16*(2), 119–128.

Hetzer, M. (1987, June). The coal demon of Deep River. *The State* Magazine, 1987.

Jacobson, P. T. (2011). *Mapping and assessment of the United States ocean wave energy resource.* Electric Power Research Institute.

Kalbfleisch, J. D., & Prentice, R. L. (2011). *The statistical analysis of failure time data*. Hoboken, NJ: John Wiley & Sons.

Leaman, K. D., Johns, E., & Rossby, T. (1989). The average distribution of volume transport and potential vorticity with temperature at three sections across the Gulf Stream. *Journal of Physical Oceanography, 19*(1), 36–51.

Lun, I. Y., & Lam, J. C. (2000). A study of Weibull parameters using long-term wind observations. *Renewable Energy, 20*(2), 145–153.

Marais, E., Chowdhury, S., & Chowdhury, S. A. (2011). *Theoretical resource assessment of marine current energy in the Agulhas Current along South Africa's East coast*. Power and Energy Society General Meeting, 2011 IEEE, IEEE.

Minerals Management Service. (2006, May). *Technology white paper on wind energy potential on the U.S. outer continental shelf.* Washington, DC: U.S. Department of the Interior.

Musial, W., & Ram, B. (2010). *Large-scale offshore wind power in the United States: Assessment of opportunities and barriers.* Golden, CO: National Renewable Energy Laboratory (NREL).

OPEC states declare oil embargo. (2014). *The History Channel website*. Retrieved May 18, 2014, from http://www.history.com/this-day-in-history/opec-states-declare-oil-embargo.

OTEC International. (2011). *OTEC History.* Retrieved May 18, 2014, from http://www.oteci.com/otec-at-work/test-page

Perlin, J. (1999). *From space to earth: The story of solar electricity.* Ann Arbor, MI: aatec Publishers.

Rajagopalan, K. (2013). An assessment of global ocean thermal energy conversion resources with a high-resolution ocean general circulation model. *Journal of Energy Resources Technology, 135*(4), 041202.

Saenko, A. V. (2008). *Assessment of wind energy resources for residential use in Victoria, BC, Canada* (Master's Thesis, University of Victoria, Victoria, BC).

Safari, B., & Gasore, J. (2010). A statistical investigation of wind characteristics and wind energy potential based on the Weibull and Rayleigh models in Rwanda. *Renewable Energy, 35*(12), 2874–2880.

Schwartz, M. N., Heimiller, D., Haymes, S., & Musial, W. (2010). *Assessment of offshore wind energy resources for the United States*. Golden, CO: National Renewal Energy Laboratory.

Scruggs, J., & Jacob, P. (2009). Harvesting ocean wave energy. *Science, 323*(5918), 1176–1178.

Smentek-Duerr, A. E. (2012). *A hydrokinetic resource assessment of the Florida Current.* Florida Atlantic University.

Sweet, C. (2012, June 13). U.S. solar-panel demand expected to double. *Wall Street Journal (Online)*. Retrieved from http://search.proquest.com/docview/1020028814?accountid=12711

Uchida, R. N. (1983). *Summary of pertinent biological characteristics of potential ocean thermal energy conversion (OTEC) sites in the Pacific Ocean.* Honolulu, HI: Southwest Fisheries Center Honolulu Laboratory, National Marine Fisheries Service.

U.S. Energy Information Administration (EIA), *Electric Power Monthly*, March 2013

U.S. Department of Energy. (n.d.). *History of hydropower.* Washington, DC: Office of Energy Efficiency & Renewable Energy. Retrieved May 18, 2014, from http://energy.gov/eere/water/history-hydropower

Vanek, F. M., & Albright, L. D. (2008). *Energy systems engineering: Evaluation & implementation.* New York, NY: McGraw-Hill.

Von Arx, W. S., Stewart, H. B., Jr., & Apel, J. R. (1974, February). *The Florida Current as a potential source of useable energy*. Proceedings of the MacArthur Workshop on the Feasibility of Extracting Useable Energy from the Florida Current, February.

Wilburn, D. R. (2011). *Wind energy in the United States and materials required for the land-based wind turbine industry from 2010 through 2030*. US Geological Survey Scientific Investigations Report 2011-5036..

Wright, S. H., Chowdhury, S. P., & Chowdhury, S. (2011). *A feasibility study for marine energy extraction from the Agulhas Current.* 2011 IEEE Power and Energy Society General Meeting, San Diego, CA.

Yang, X. (2013). Ocean current energy resource assessment for the United States.

Appendix A

Additional Figures from Velocity Analysis

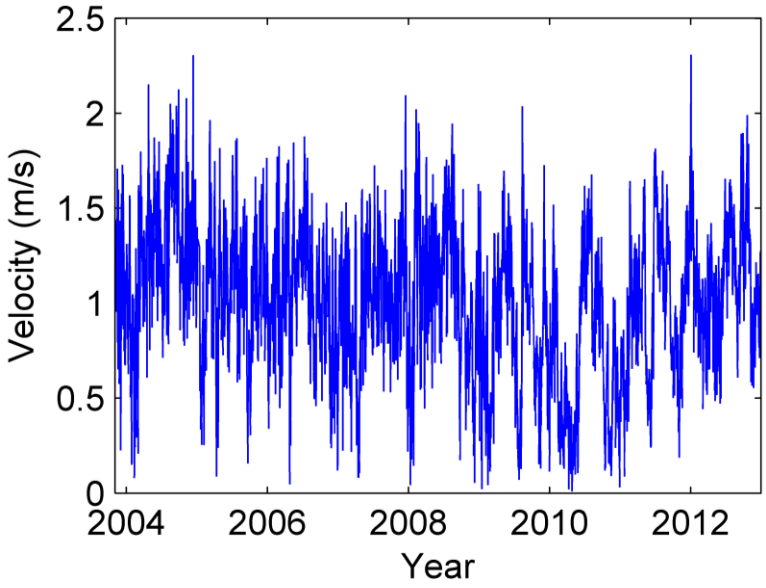

Figure A-1. Daily average of ocean current velocity at a depth of 20m at point A1 between 2004 and 2012 (HYCOM).

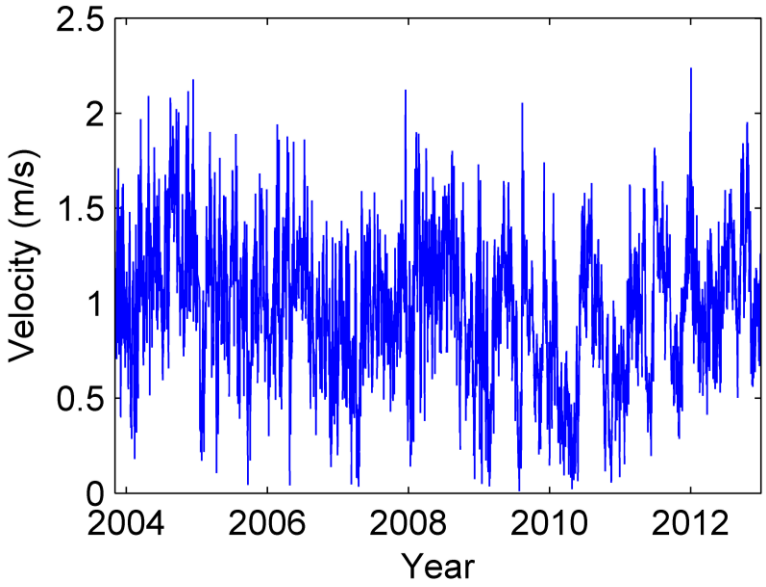

Figure A-2. Daily average of ocean current velocity at a depth of 20m at point A2 between 2004 and 2012 (HYCOM).

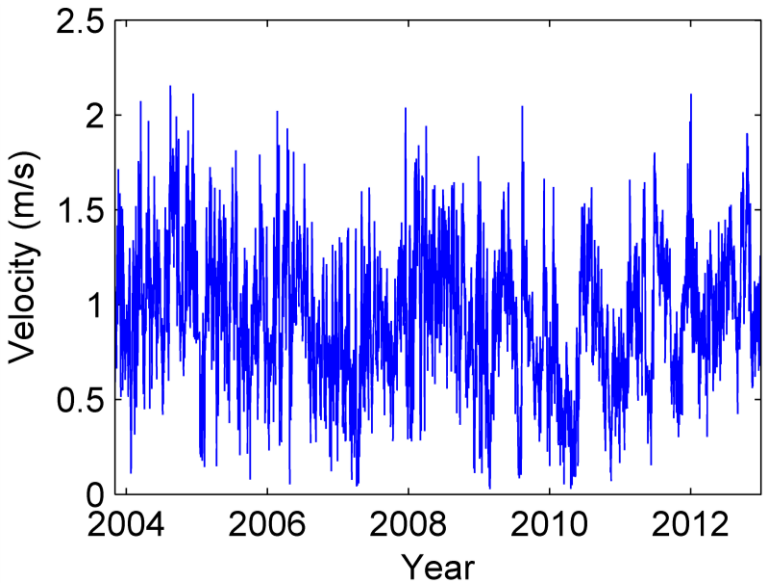

Figure A-3. Daily average of ocean current velocity at a depth of 20m at point A3 between 2004 and 2012 (HYCOM).

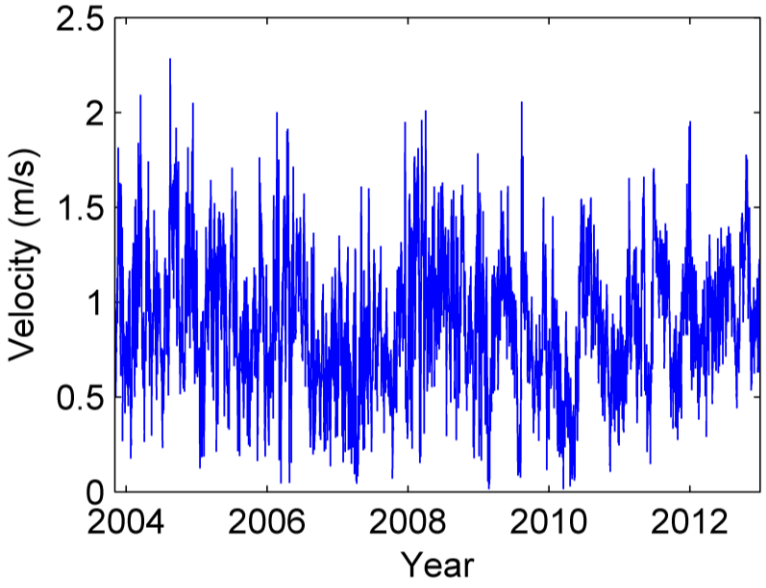

Figure A-4. Daily average of ocean current velocity at a depth of 20m at point A4 between 2004 and 2012 (HYCOM).

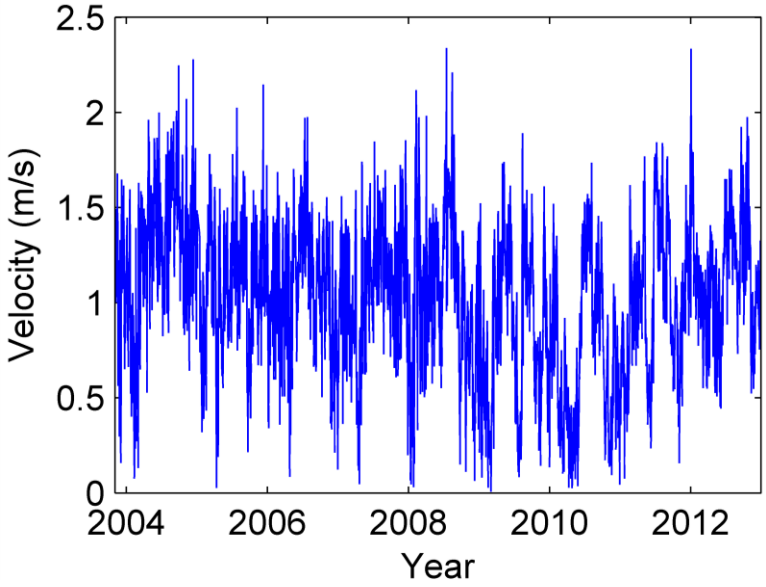

Figure A-5. Daily average of ocean current velocity at a depth of 20m at point B1 between 2004 and 2012 (HYCOM).

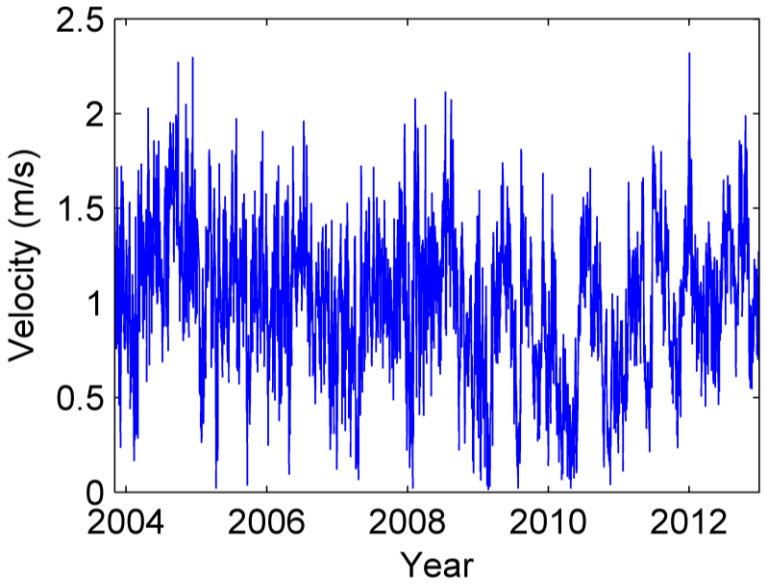

Figure A-6. Daily average of ocean current velocity at a depth of 20m at point B2 between 2004 and 2012 (HYCOM).

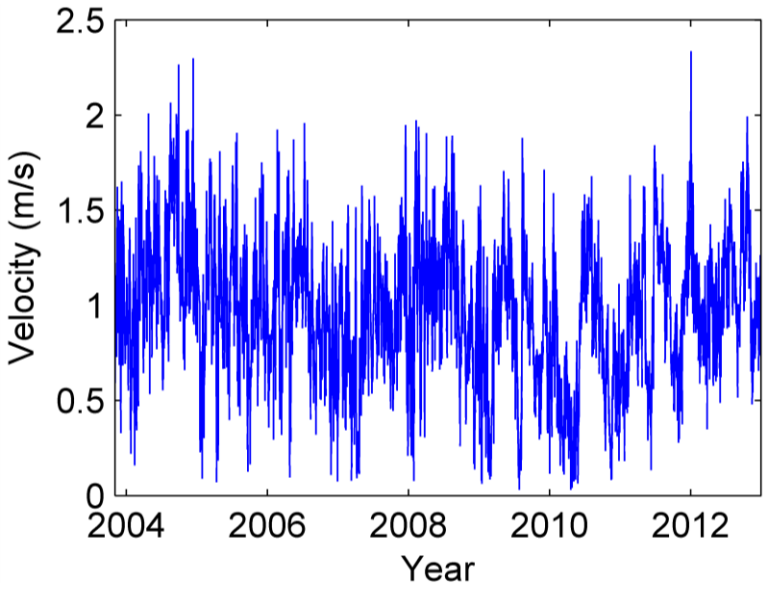

Figure A-7. Daily average of ocean current velocity at a depth of 20m at point B3 between 2004 and 2012 (HYCOM).

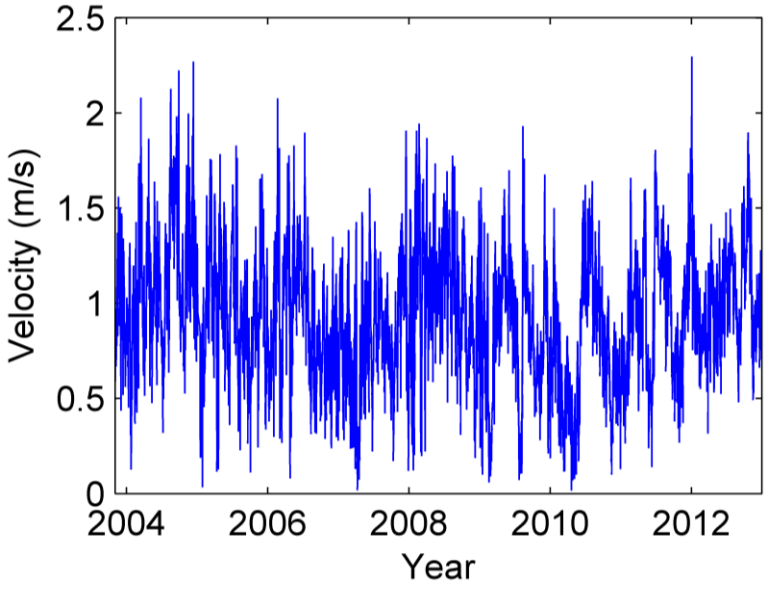

Figure A-8. Daily average of ocean current velocity at a depth of 20m at point B4 between 2004 and 2012 (HYCOM).

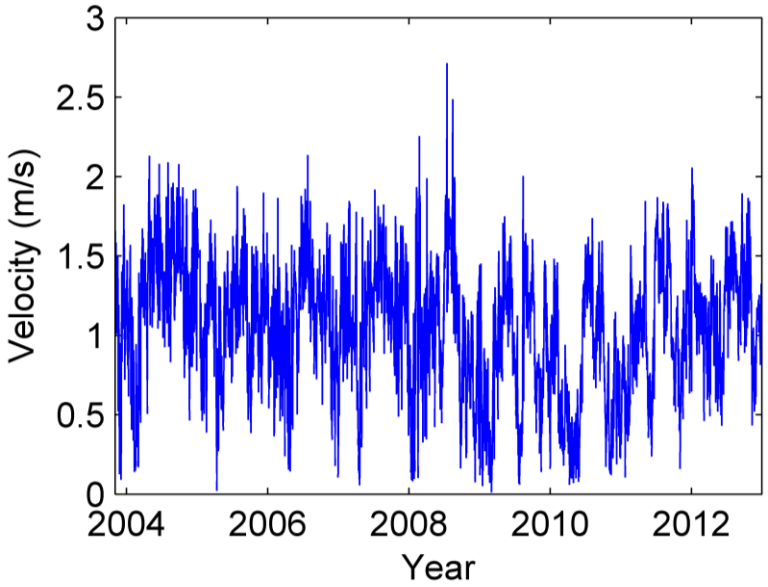

Figure A-9. Daily average of ocean current velocity at a depth of 20m at point C1 between 2004 and 2012 (HYCOM).

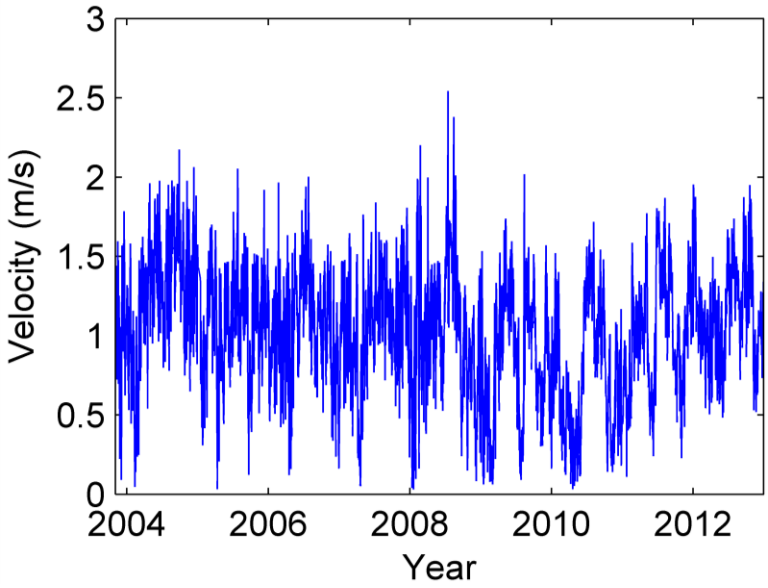

Figure A-10. Daily average of ocean current velocity at a depth of 20m at point C2 between 2004 and 2012 (HYCOM).

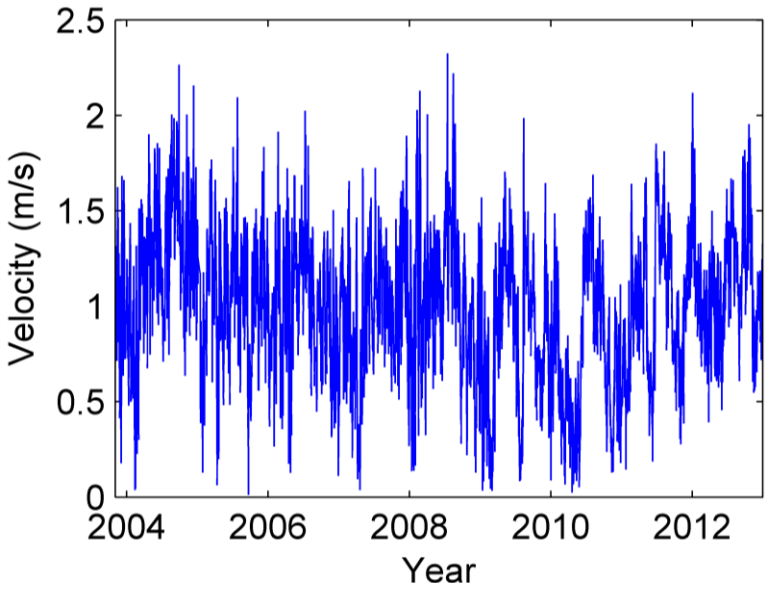

Figure A-11. Daily average of ocean current velocity at a depth of 20m at point C3 between 2004 and 2012 (HYCOM).

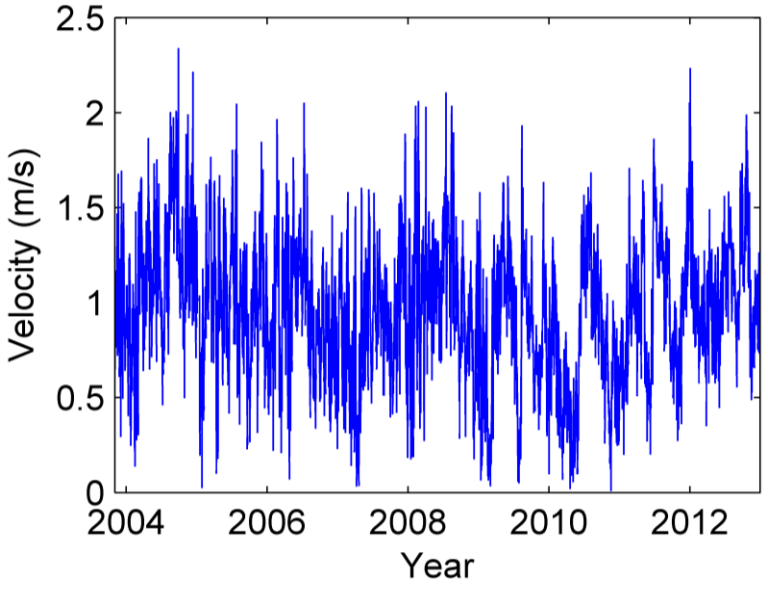

Figure A-12. Daily average of ocean current velocity at a depth of 20m at point C4 between 2004 and 2012 (HYCOM).

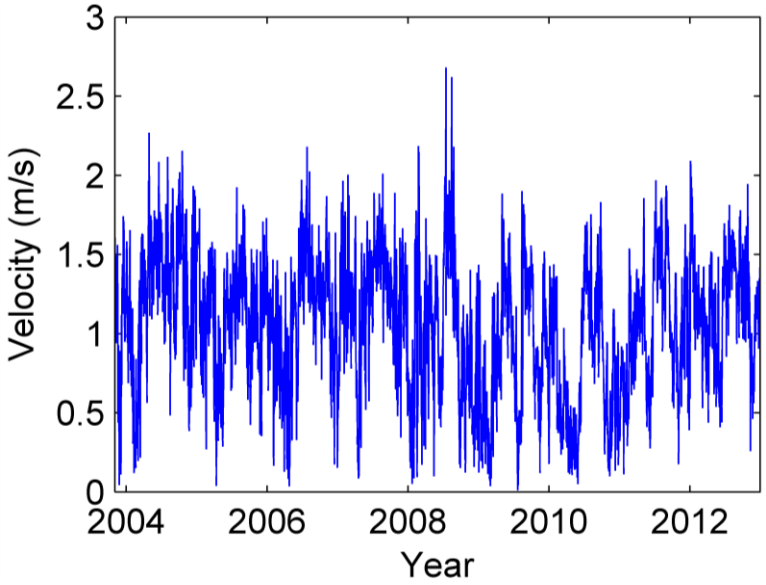

Figure A-13. Daily average of ocean current velocity at a depth of 20m at point D1 between 2004 and 2012 (HYCOM).

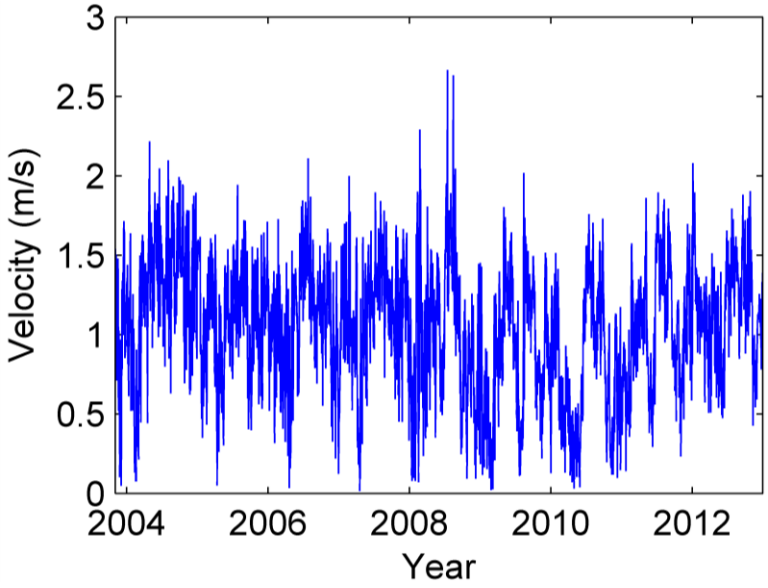

Figure A-14. Daily average of ocean current velocity at a depth of 20m at point D2 between 2004 and 2012 (HYCOM).

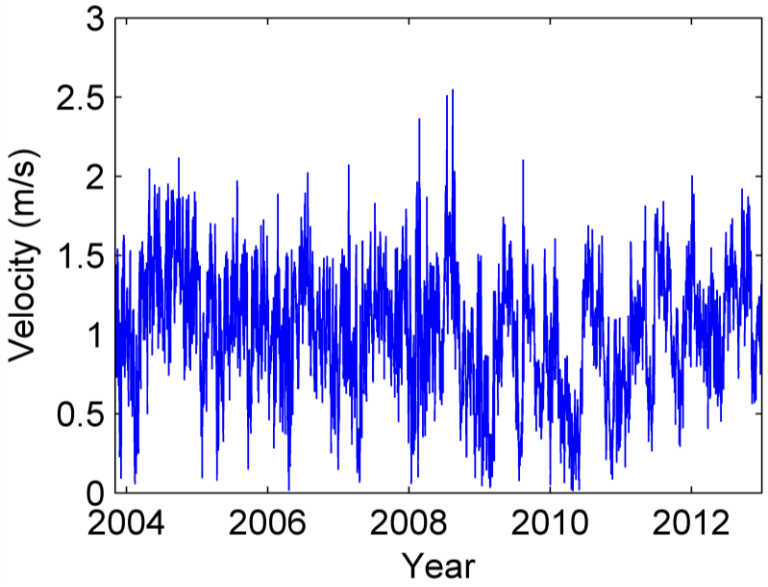

Figure A-15. Daily average of ocean current velocity at a depth of 20m at point D3 between 2004 and 2012 (HYCOM).

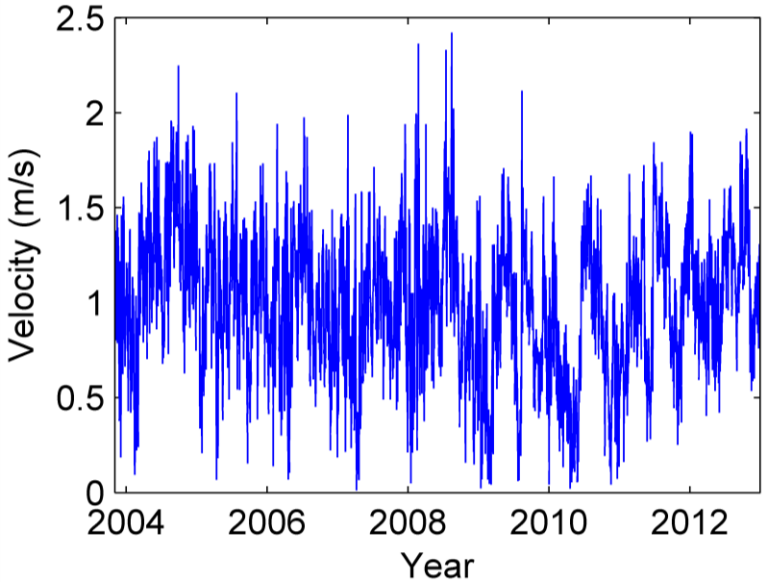

Figure A-16. Daily average of ocean current velocity at a depth of 20m at point D4 between 2004 and 2012 (HYCOM).

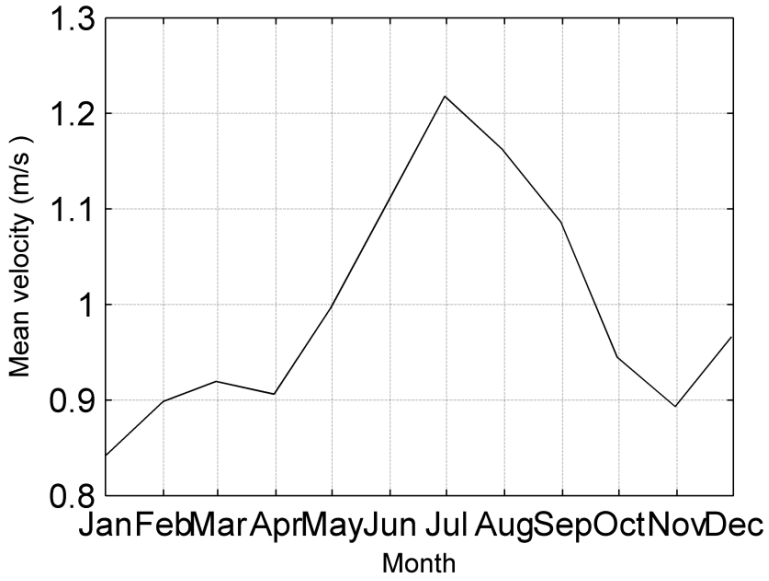

Figure A-17. Monthly mean velocity at A1 for the entire period (HYCOM).

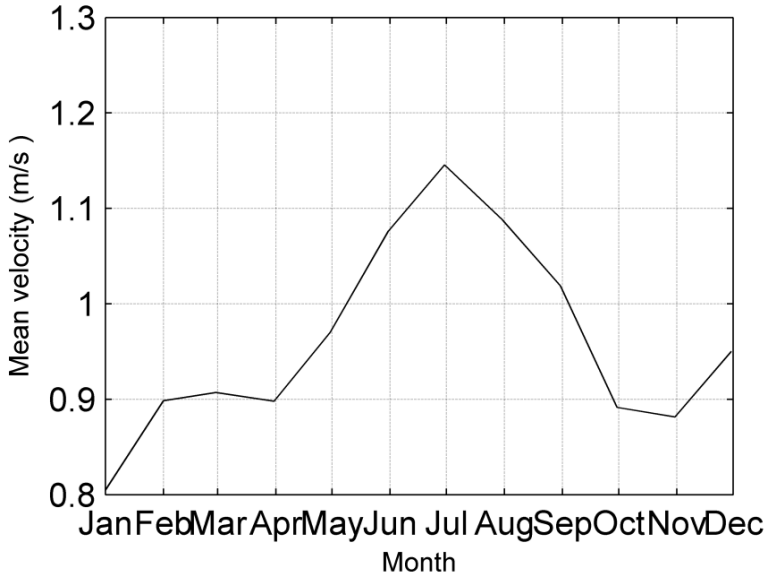

Figure A-18. Monthly mean velocity at A2 for the entire period (HYCOM).

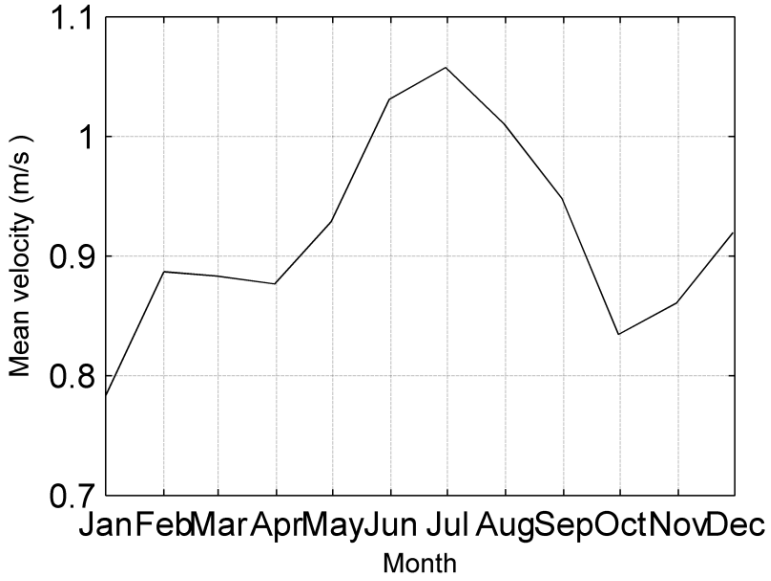

Figure A-19. Monthly mean velocity at A3 for the entire period (HYCOM).

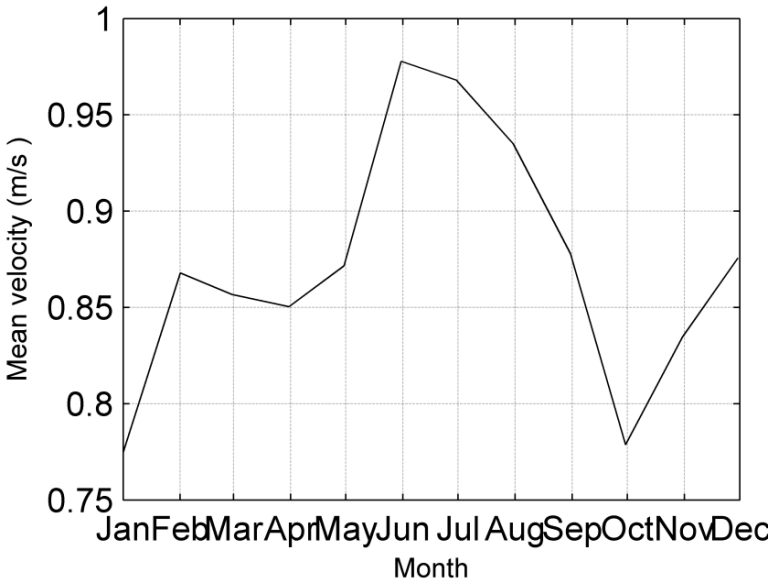

Figure A-20. Monthly mean velocity at A4 for the entire period (HYCOM).

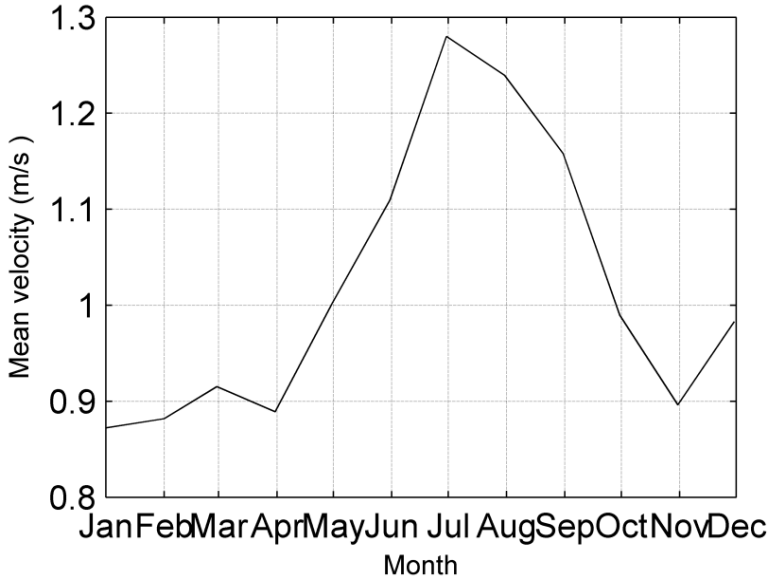

Figure A-21. Monthly mean velocity at B1 for the entire period (HYCOM).

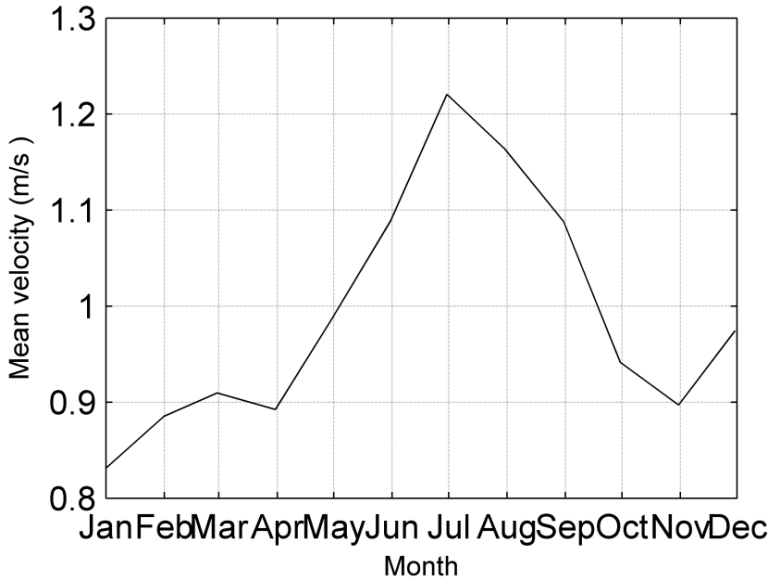

Figure A-22. Monthly mean velocity at B2 for the entire period (HYCOM).

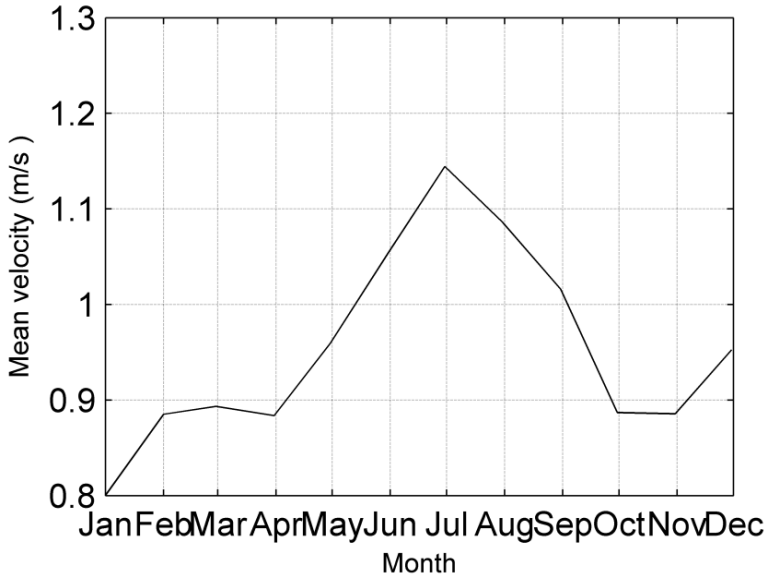

Figure A-23. Monthly mean velocity at B3for the entire period (HYCOM).

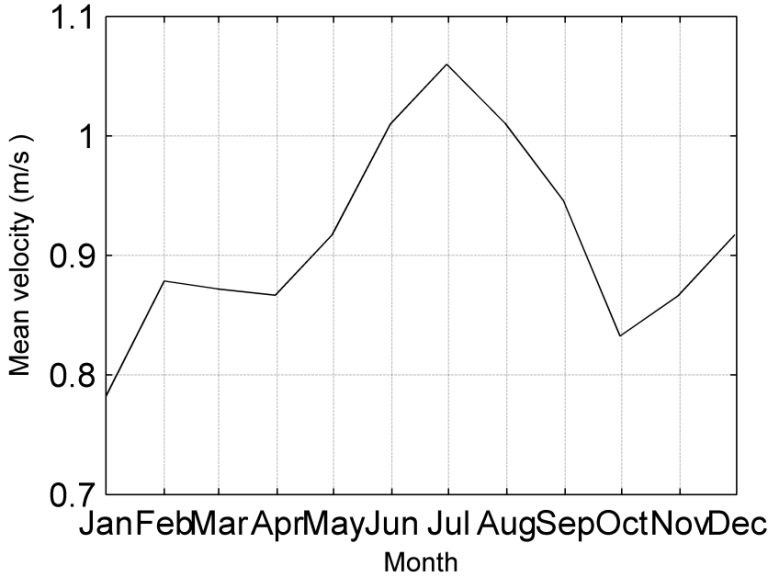

Figure A-24. Monthly mean velocity at B4for the entire period (HYCOM).

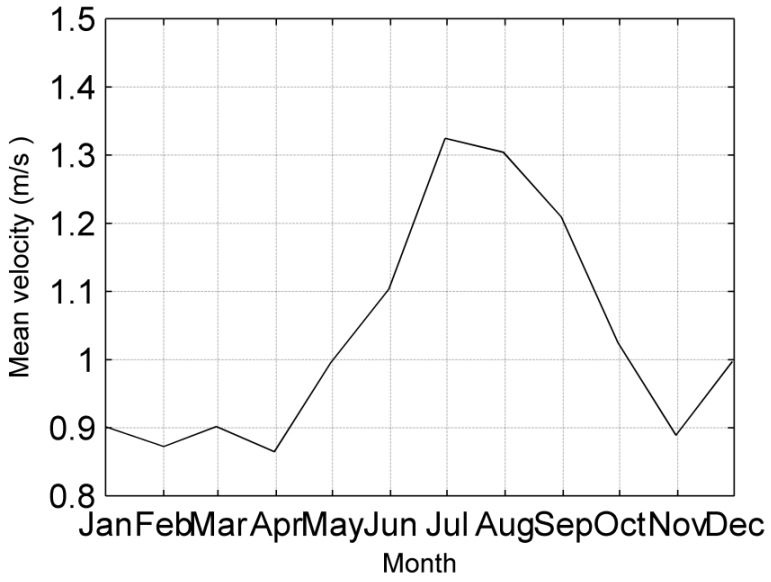

Figure A-25. Monthly mean velocity at C1 for the entire period (HYCOM).

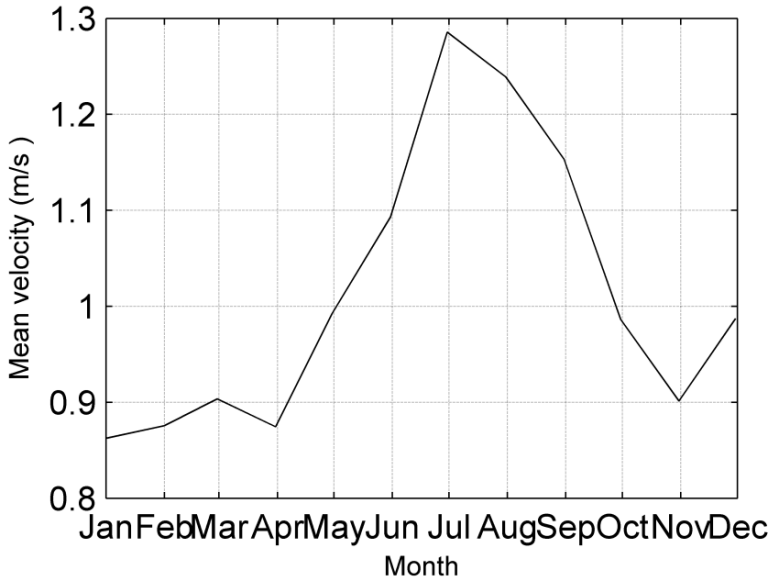

Figure A-26. Monthly mean velocity at C2 for the entire period (HYCOM).

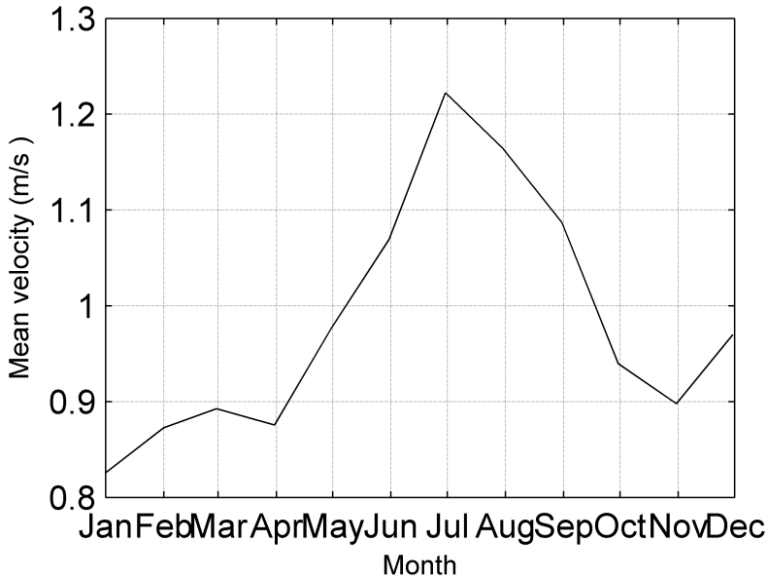

Figure A-27. Monthly mean velocity at C3 for the entire period (HYCOM).

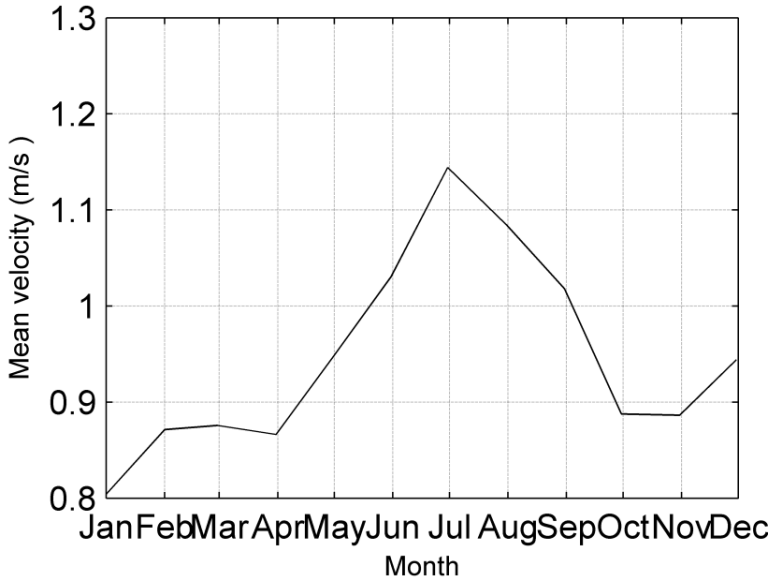

Figure A-28. Monthly mean velocity at C4 for the entire period (HYCOM).

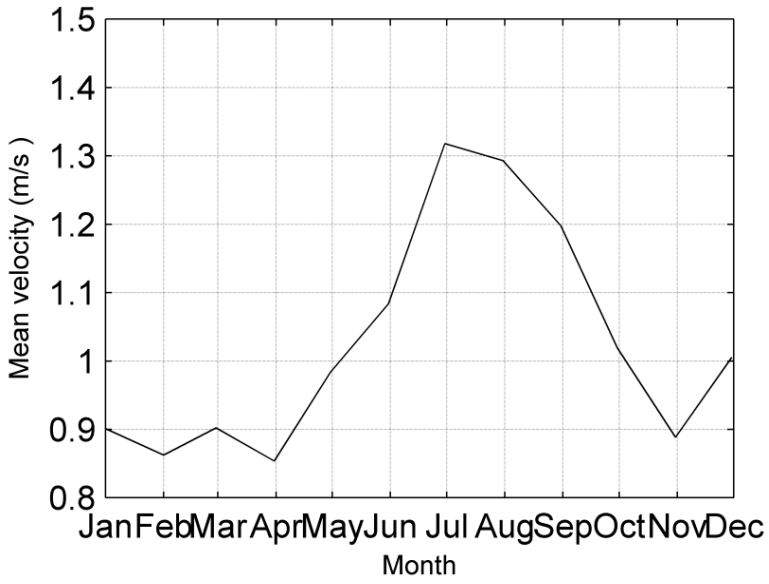

Figure A-29. Monthly mean velocity at D2 for the entire period (HYCOM).

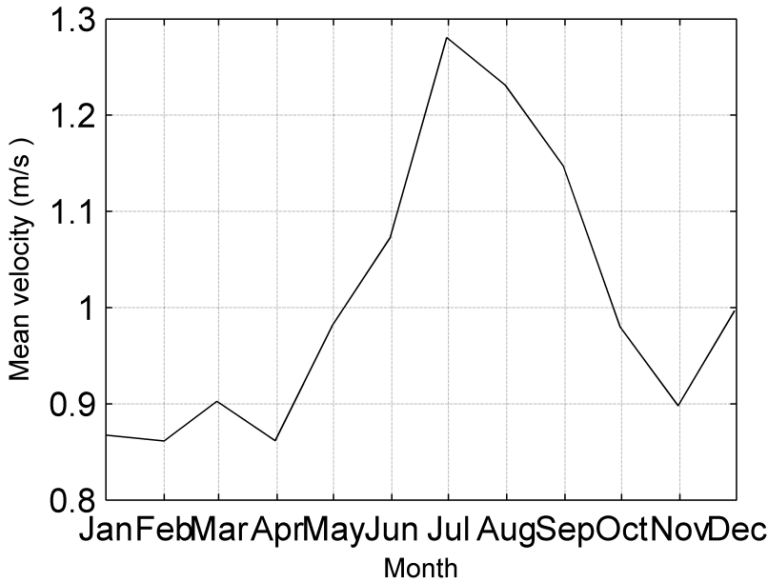

Figure A-30. Monthly mean velocity at D3 for the entire period (HYCOM).

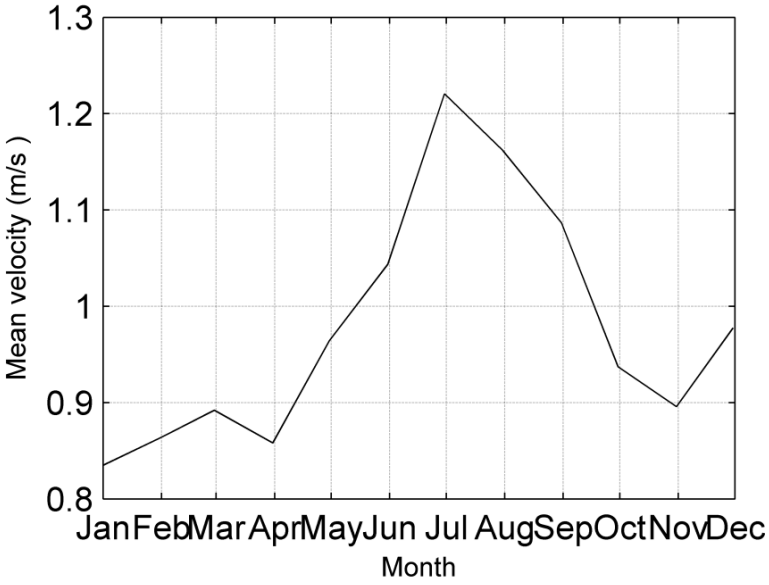

Figure A-31. Monthly mean velocity at D4for the entire period (HYCOM).

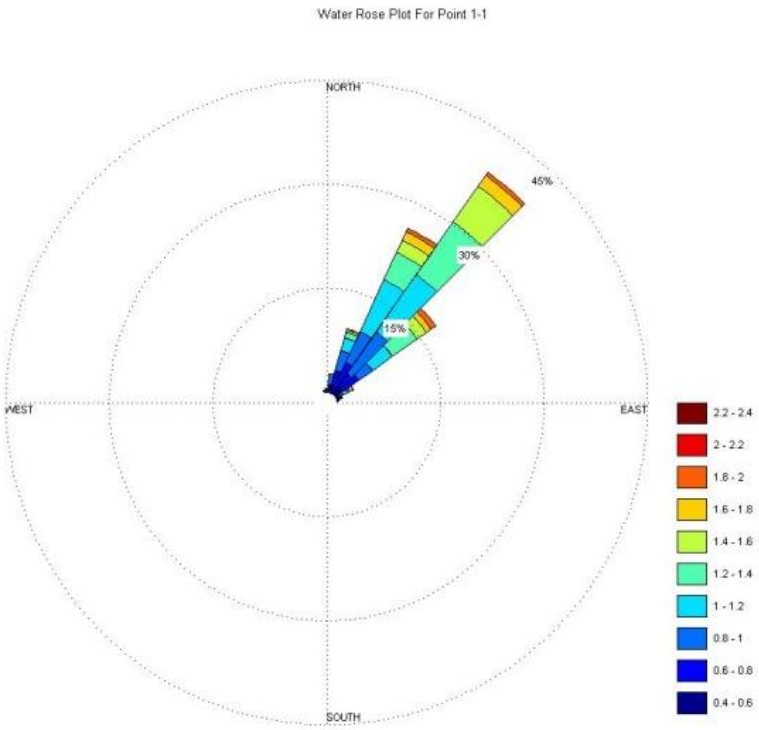

Figure A-32. Rose Plots for Ocean Current velocity at A1.

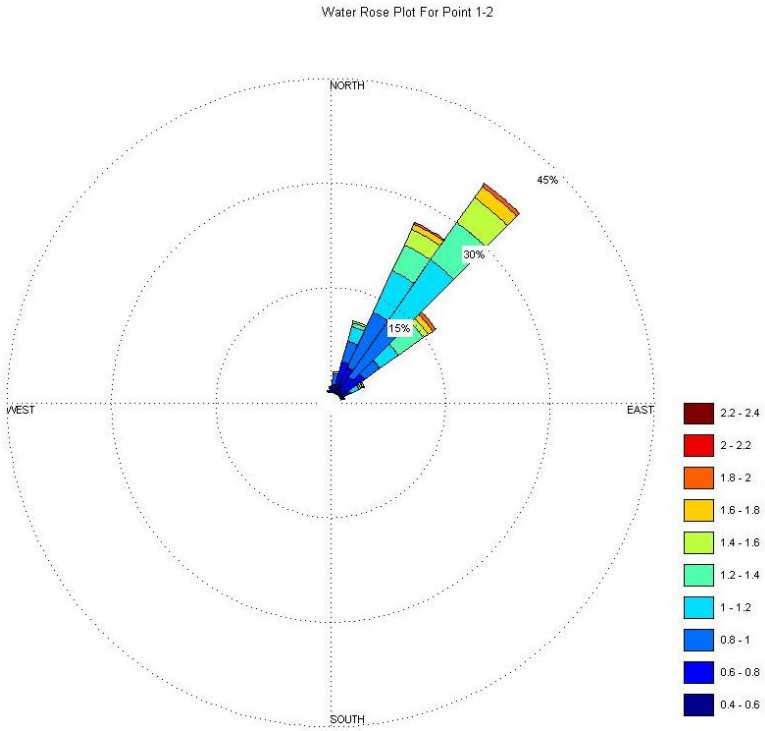

Figure A-33. Rose Plots for Ocean Current velocity at A2.

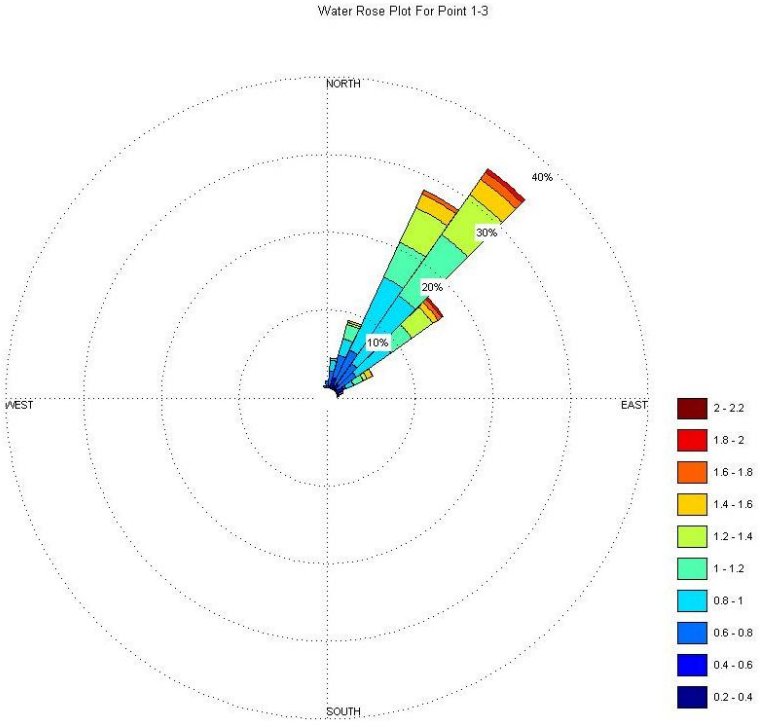

Figure A-34. Rose Plots for Ocean Current velocity at A3.

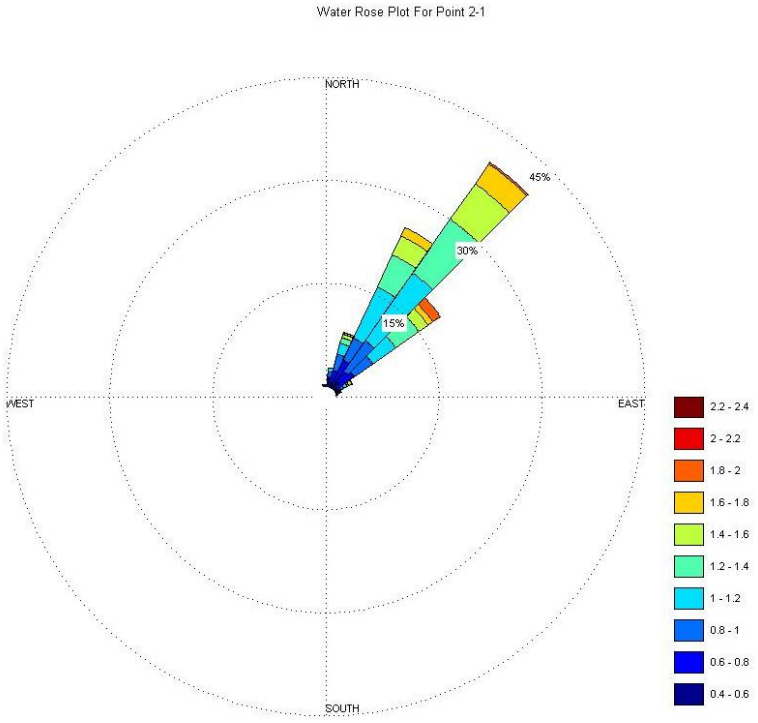

Figure A-35. Rose Plots for Ocean Current velocity at B1.

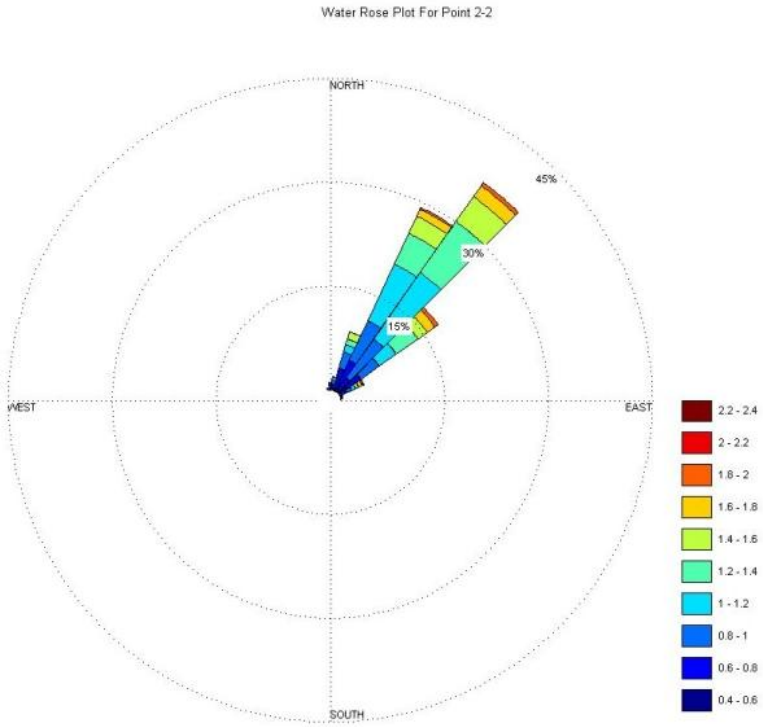

Figure A-36. Rose Plots for Ocean Current velocity at B2.

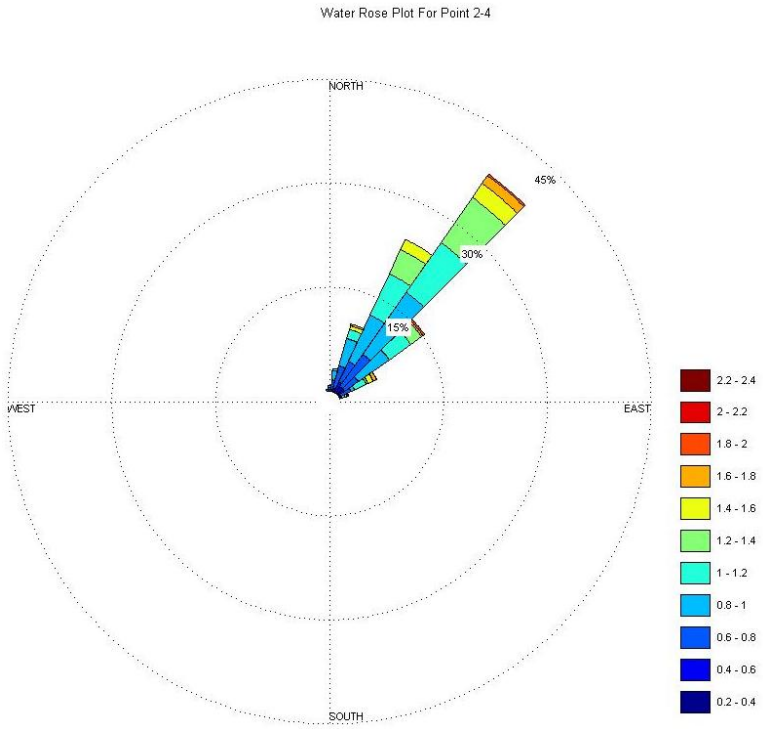

Figure A-37. Rose Plots for Ocean Current velocity at B4.

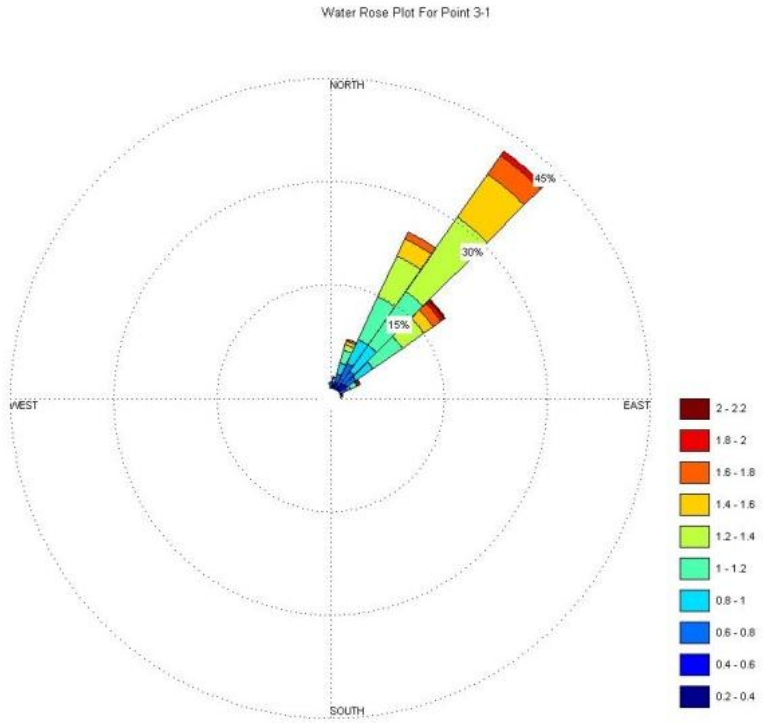

Figure A-38. Rose Plots for Ocean Current velocity at C1.

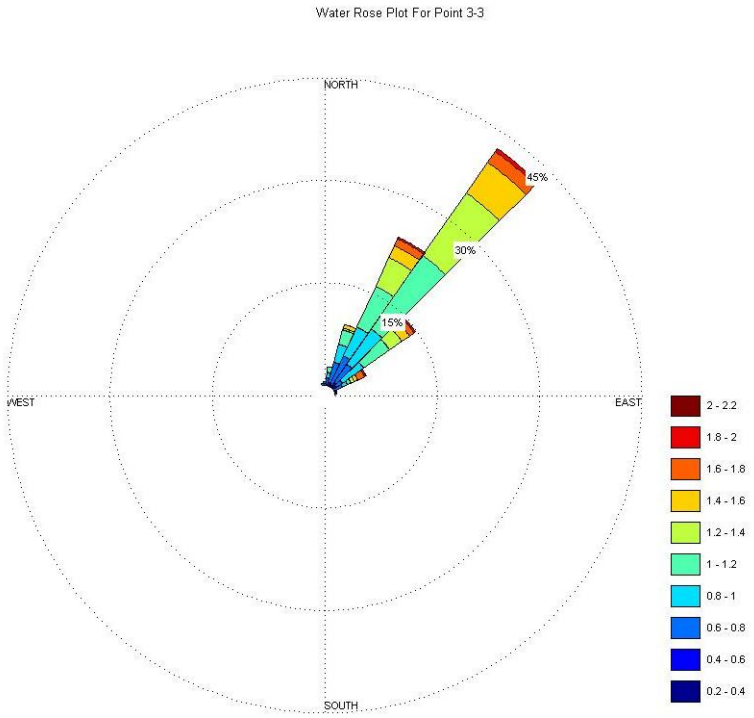

Figure A-39. Rose Plots for Ocean Current velocity at C3.

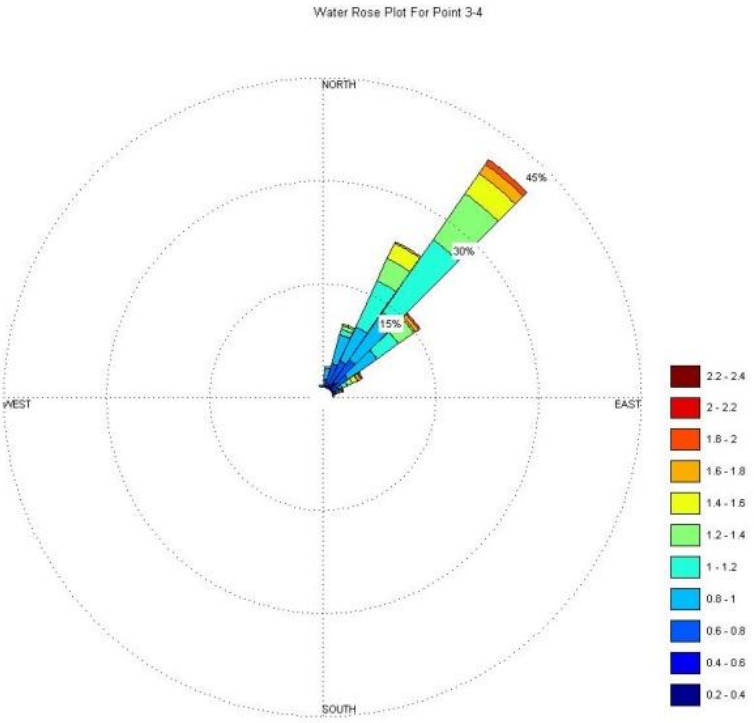

Figure A-40. Rose Plots for Ocean Current velocity at C4.

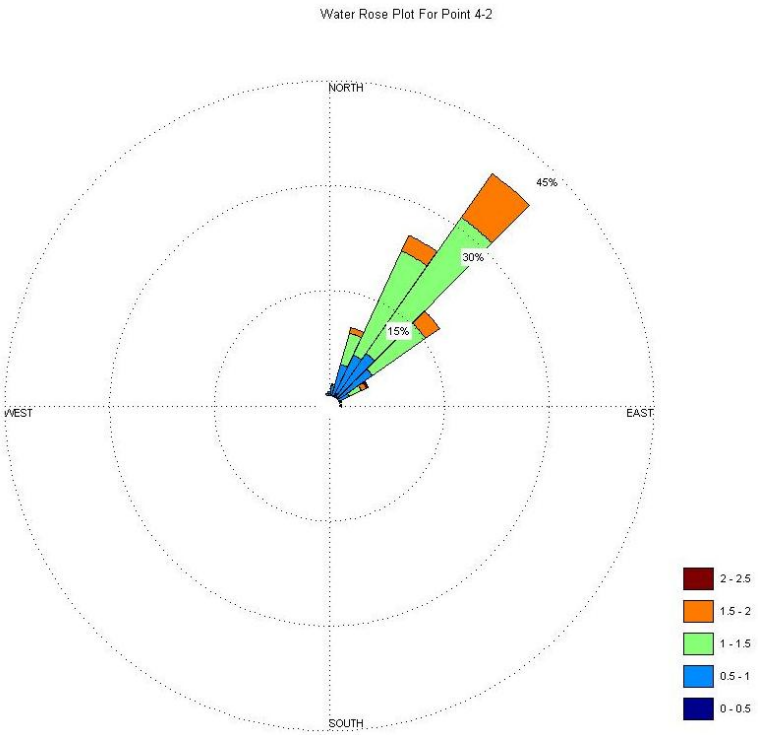

Figure A-41. Rose Plots for Ocean Current velocity at D2.

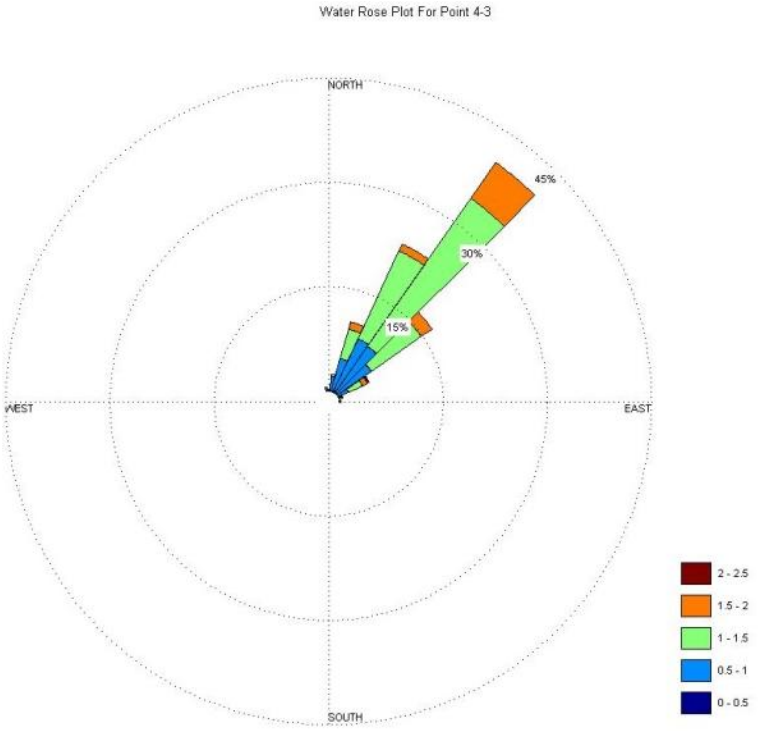

Figure A-42. Rose Plots for Ocean Current velocity at D3.

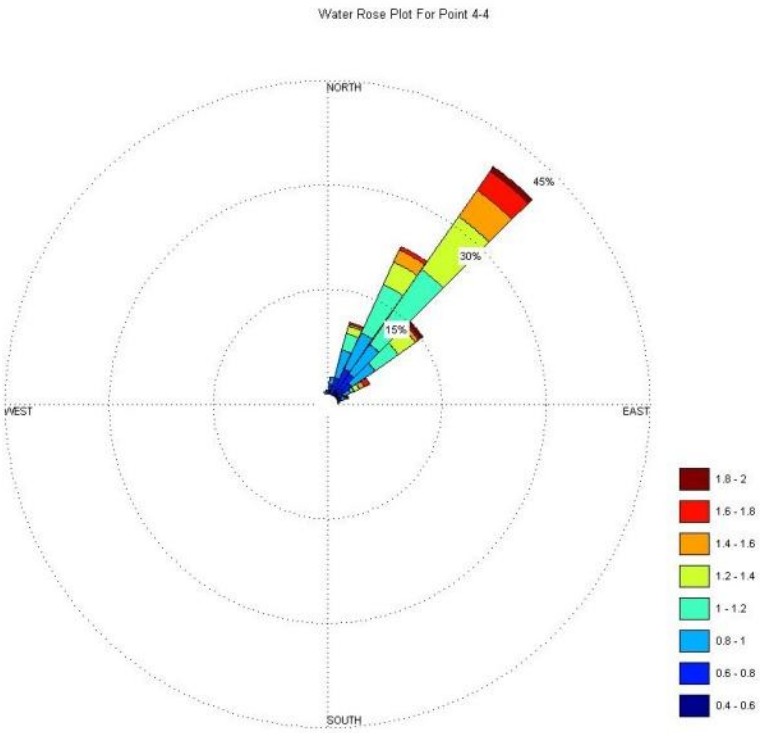

Figure A-43. Rose Plots for Ocean Current velocity at D3.

Appendix B

Additional Figures and Tables from Statistical Analysis

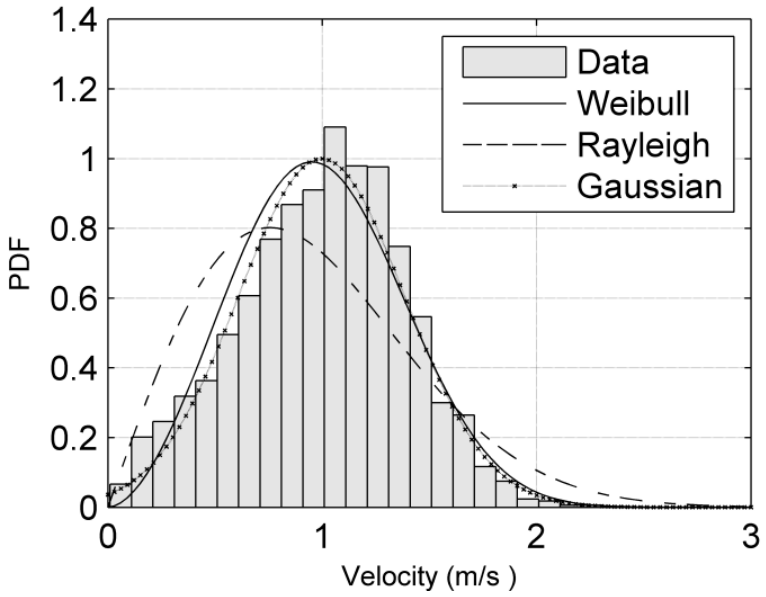

Figure B-1. Ocean current velocity histogram and predictions from the probability density functions at A1.

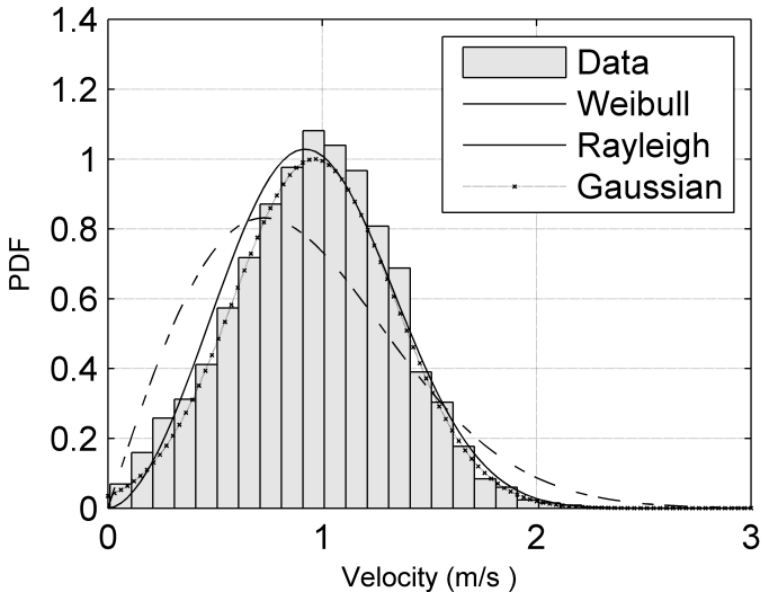

Figure B-2. Ocean current velocity histogram and predictions from the probability density functions at A2.

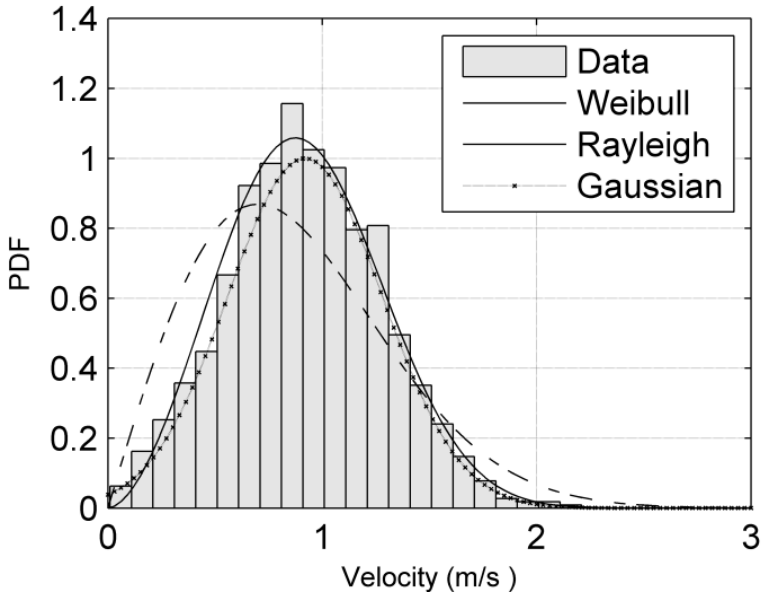

Figure B-3. Ocean current velocity histogram and predictions from the probability density functions at A3.

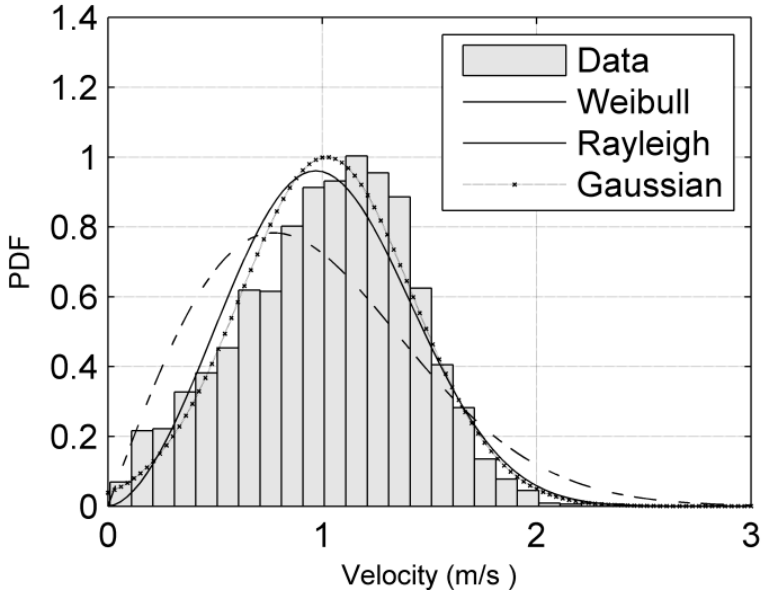

Figure B-4. Ocean current velocity histogram and predictions from the probability density functions at B1.

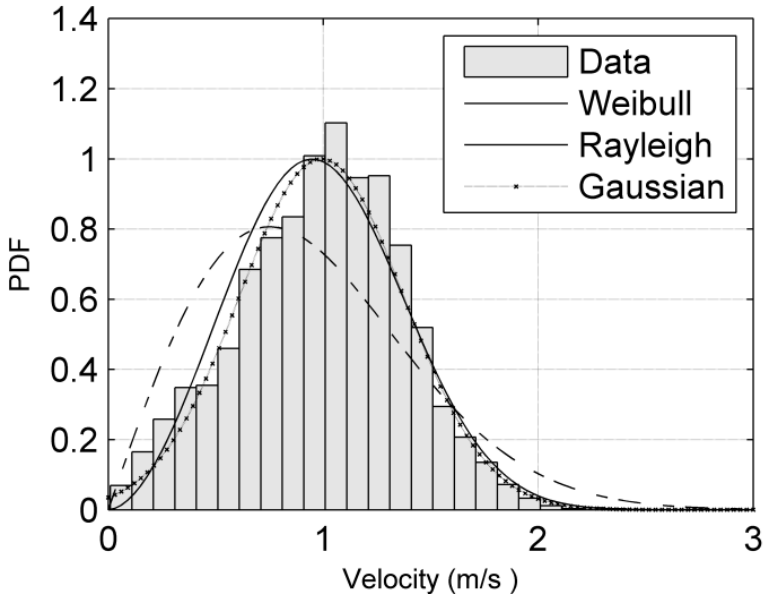

Figure B-5. Ocean current velocity histogram and predictions from the probability density functions at B2.

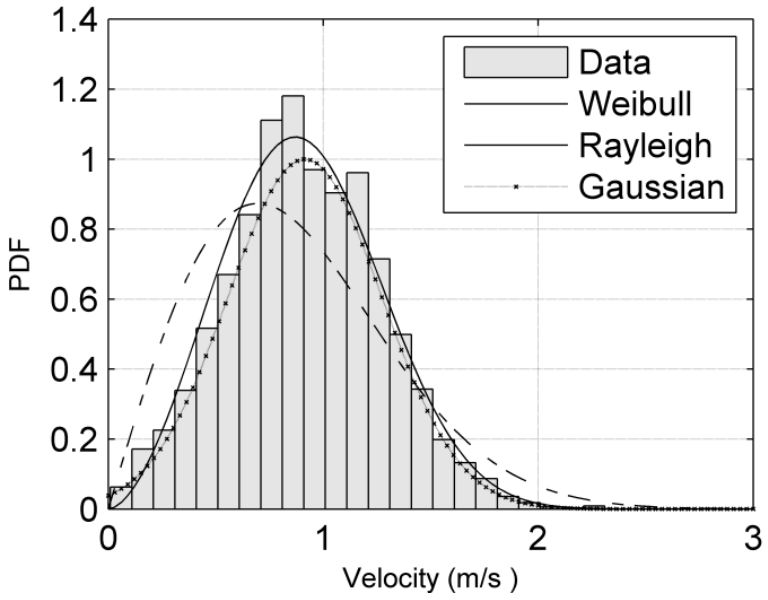

Figure B-6. Ocean current velocity histogram and predictions from the probability density functions at B4.

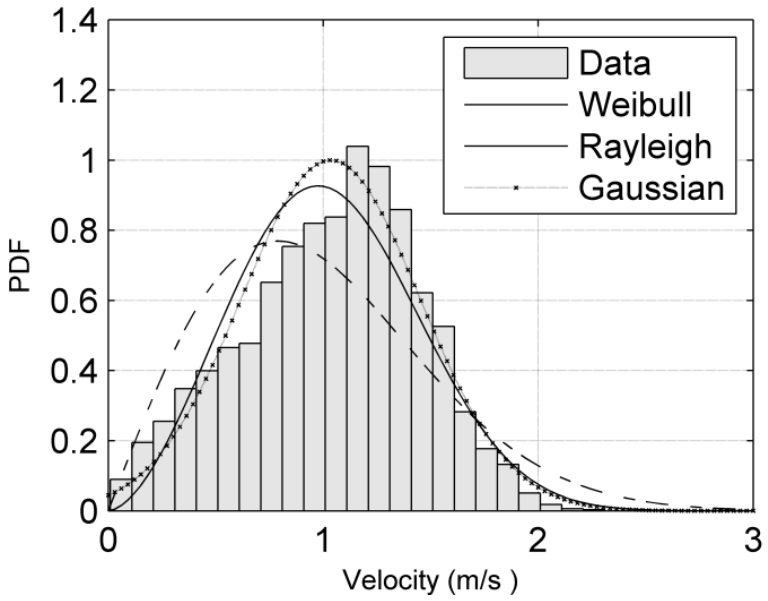

Figure B-7. Ocean current velocity histogram and predictions from the probability density functions at C1.

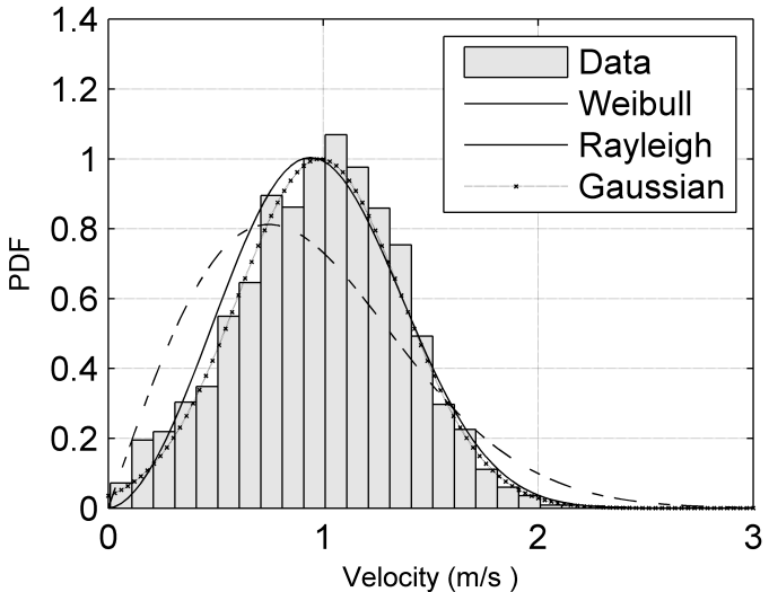

Figure B-8. Ocean current velocity histogram and predictions from the probability density functions at C3.

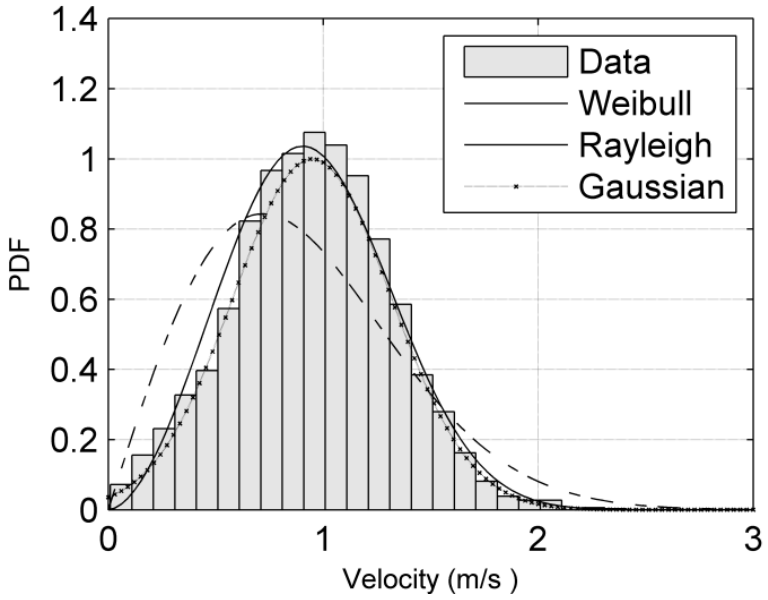

Figure B-9. Ocean current velocity histogram and predictions from the probability density functions at C4.

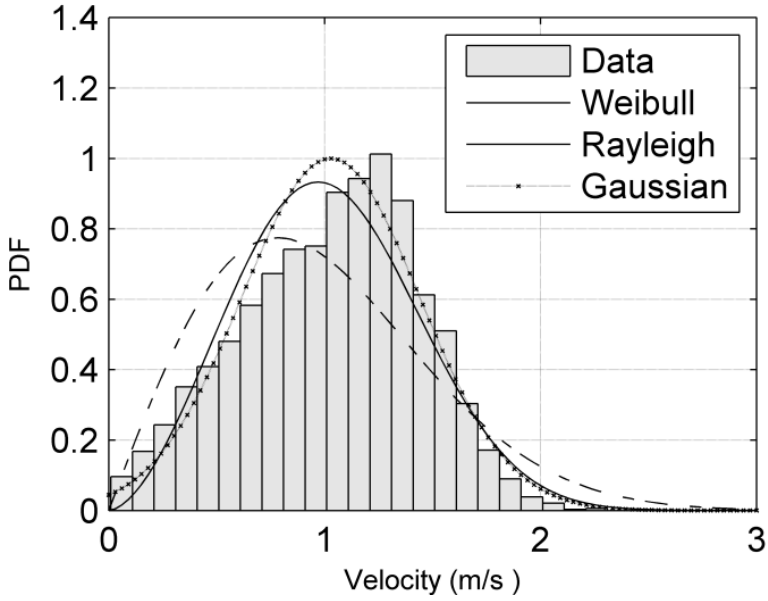

Figure B-10. Ocean current velocity histogram and predictions from the probability density functions at D2.

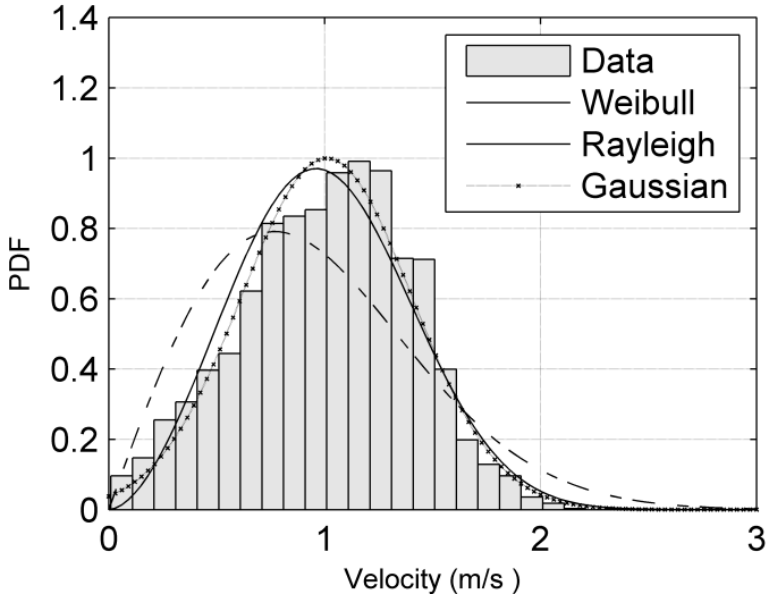

Figure B-11. Ocean current velocity histogram and predictions from the probability density functions at D3.

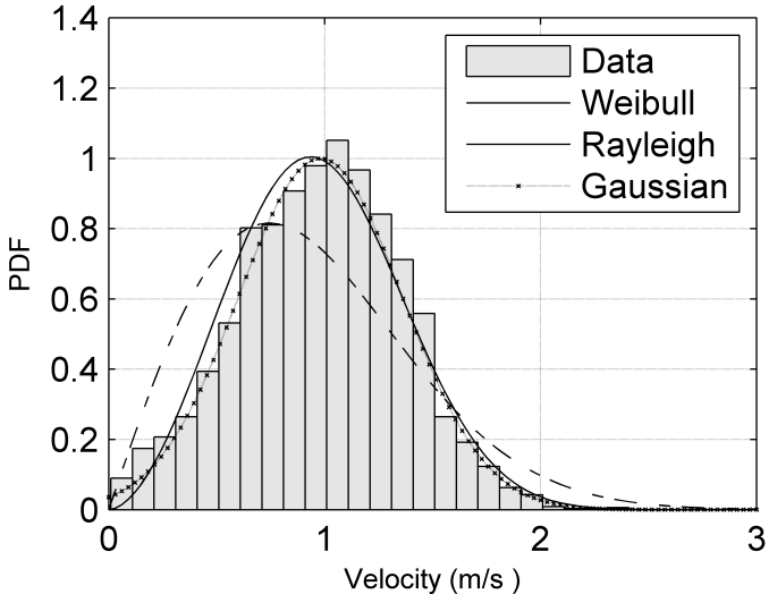

Figure B-12. Ocean current velocity histogram and predictions from the probability density functions at D4.